THE JOHNS HOPKINS UNIVERSITY

DEPARTMENT OF PHYSICS

Final Report

A STUDY OF THE FEASIBILITY OF ULTRAVIOLET SPECTROMETRY FOR COMETARY MISSIONS

Paul D. Feldman, Principal Investigator

Prepared under

National Aeronautics and Space Administration

NSG

Grant 7382

February 28, 1979

Baltimore, Maryland 21218

FINAL REPORT

A STUDY OF THE FEASIBILITY OF ULTRAVIOLET SPECTROMETRY FOR COMETARY MISSIONS

NASA Grant NSG 7382

Prepared by: Paul D. Feldman
Physics Department
Johns Hopkins University
Baltimore, MD 21218

February 28, 1979

TABLE OF CONTENTS

I. Introduction

Ultraviolet spectroscopy has proven to be an extremely valuable source of information about the atmospheres of the earth and planets. The reasons for this are largely fortuitous -- the principal constituents of these atmospheres are the basic atoms H, C, N and O or simple molecules formed from these atoms such as N_2, O_2, CO_2, H_2, etc. and these species largely have their strongest electronic transitions in the vacuum ultraviolet. Furthermore, in many cases the sun emits strongly at the same wavelengths so that the efficiency for resonance scattering or fluorescence in these transitions is high while at the same time the low solar continuum below 1800 Å permits observation of these lines against the full disk of the planet. Observations of ultraviolet spectra of planets have been made mainly by sounding rocket (Venus, Jupiter, Saturn), planetary fly-by (Mariners to Venus, Mercury and Mars, Pioneer Jupiter) and orbiter (Mariner 9 - Mars).

The same techniques are applicable to the study of cometary atmospheres since most of what we see when we observe a comet is the atmosphere. In contrast to the planets where the atmospheric scale heights are much smaller than the planet's radius, a comet has a "solid" nucleus of the order of 10 km and an atmospheric scale length determined by the lifetimes of the constituent species in the solar radiation field, typically of the order of 10^5 - 10^6 km at 1 a.u. Unlike any planet, the cometary atmosphere or "coma", is not bound by gravity, has no appreciable magnetic field, can have a large component of micron size dust particles, and is principally composed of water vapor and its dissociation products, H, O and OH. Although OH had been observed for many years from the ground via the (0,0) band of the $^2\Sigma^+ \rightarrow X^2\Pi$ transition near 3090 Å, because of the severe attenuation by ozone at this wavelength, the

large abundance of OH, and hence of H_2O, was not recognized until the first space observations, of Comet Bennett (1970 II) in 1970. The icy conglomerate model of Whipple (1950), in which water ice is proposed as the major constituent of the cometary nucleus, was based on dynamical and thermodynamic evidence, rather than on spectroscopic data.

Because of the infrequent and random nature of apparitions of bright comets, the number of observations of such comets from space platforms is extremely limited, and, of course, it is impossible to repeat an observation at a later date. Around 1970, comets Tago-Sato-Kosaka (1969IX), Bennett, and p/Encke were observed in the light of hydrogen Lyman-α at 1216 Å, variously by OGO-5 (Bertaux et al, 1973), OAO-2 (Keller and Lillie, 1974, 1978) and by sounding rocket (Jenkins and Wingert 1972). The OAO-2 observations of Bennett also included the aforementioned OH band near 3090 Å and demonstrated conclusively the water dissociation source of the hydrogen:

$$H_2O + h\nu \rightarrow OH + H + \text{kinetic energy}$$

$$OH + h\nu \rightarrow O + H + \text{kinetic energy}$$

Direct imaging of the extensive hydrogen envelope was accomplished by rocket (Opal et al. 1974) and Skylab (Carruthers et al. 1974) observations of comet Kohoutek (1973 XII) in early 1974. Atomic carbon and oxygen were detected spectroscopically by two rocket experiments (Feldman et al. 1974, Opal et al. 1974), again in comet Kohoutek. However, the first comprehensive ultraviolet spectra of a comet were not obtained until 1976 when comet West (1976 VI) was successfully observed by three sounding rocket experiments (Johns Hopkins, University of Colorado and Goddard Space Flight Center). In Figs. 1 and 2 the spectra of Feldman and Brune (1976) of comet West are reproduced. These spectra and their interpretation form the basis for this report.

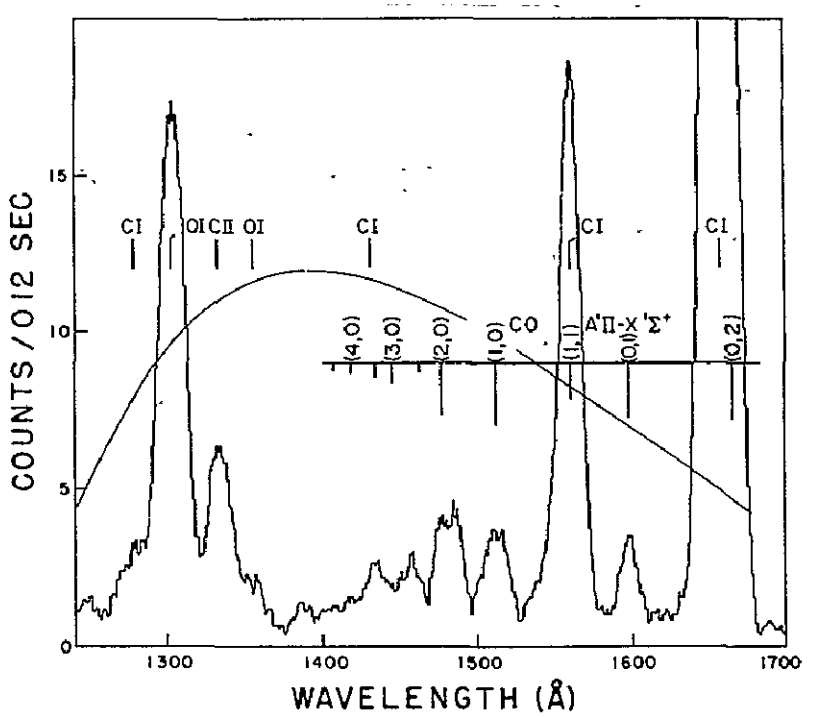

FIG. 1.—Spectrum of comet West 1975n in the 1250–1680 Å spectral range. The solid line gives the response of the spectrometer to a source of uniform spectral brightness. The peak of the C I λ1657 line is off-scale at 79 counts per 0.12 s.

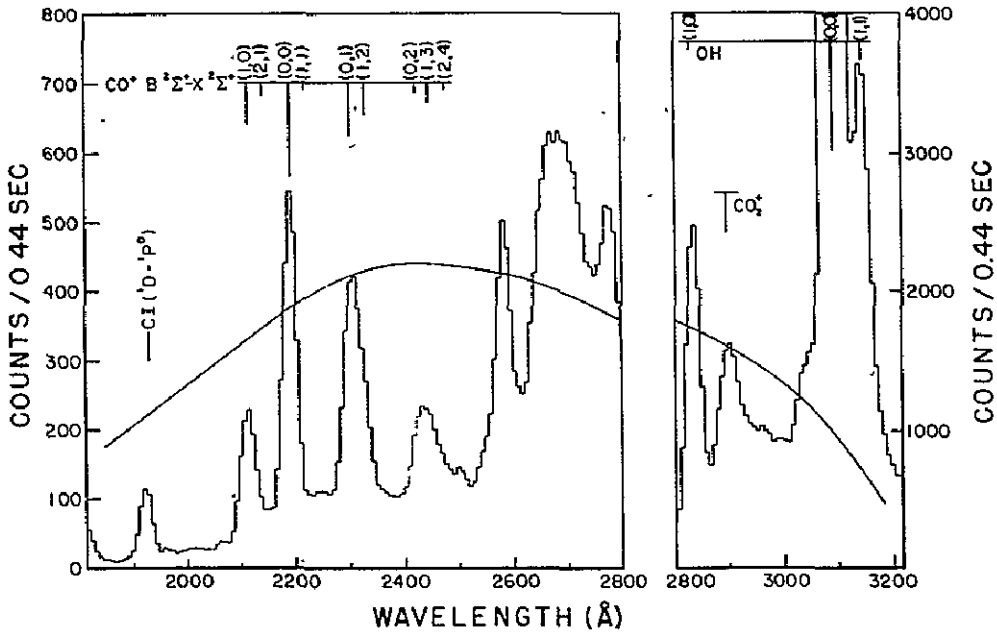

FIG. 2 —Same as Fig. 1 for the 1800–3200 Å spectral range. The off-scale value of the (0, 0) OH band is 55,000 counts per 0.44 s.

II. Objectives

The possibility of a comet mission in the early 1980s to fly-by p/Halley and subsequently rendez-vous with another comet has raised great interest and promises to provide a significant advance in our knowledge of basic cometary structure. Since an ultraviolet spectrometer is a logical candidate for such a mission it is imperative to use presently available ultraviolet data to estimate the expected brightness of the emission features of interest as well as to determine the spatial extent of these features for particular candidate missions. In practise this is done by constructing a coma model based on the observations of comet West and then evaluating the model for the physical conditions of the candidate targets such as heliocentric distance, gas production rate, composition, etc. For the particular model used, described in Section III, in addition to brightness profiles, the neutral and ion densities of the principal species are also derived. The brightness profiles can also be used to determine the feasibility of using Space Telescope to provide supporting observations during the mission. In this regard it should be noted that even the strongest emission features, HI Lyman-α and the OH (0,0) band may be difficult to observe, not because of a lack of instrument sensitivity, but due to a limiting night sky background, geocoronal and interplanetary Lyman-α for hydrogen or zodiacal light for OH.

Although ultraviolet spectrometers have flown successfully on several planetary missions, it is worthwhile to examine the characteristics of such an instrument for a comet mission in view of the very large spatial extent of the ultraviolet coma and the consequent large change in angular extent as seen from the spacecraft during the course of a fly-by or rendez-vous. Advances in the state-of-the-art technology of multi-element

ultraviolet detectors open the possibility of designing compact, sensitive imaging spectrographs which would also find many applications in earth-orbit observations of extended astronomical objects.

For comet observations, we will consider several scenarios -- the proposed Halley fly-by/Tempel 2 rendez-vous selected by the 1978 Comet Science Working Group; as well as possible Halley or Encke fly-bys close to perihelion. The objective is to identify a set of basic parameters based on the model predictions and the physical spacecraft constraints (weight, volume, power) which include:

Spectral range

Wavelength resolution

Spatial resolution

Sensitivity and dynamic range

Rejection of scattered light

Integration or accumulation times

The models, along with available dust models, can also be used to define the pointing requirements and to evaluate the potential hazard from cometary dust in a particular mission.

As noted above, an incidental result of the models is the derivation of the density profiles of the principal neutral and ion species, which should provide useful information for any mass spectrometer experiments flown.

III. The Ultraviolet Coma

The spectra of Figs. 1 and 2 confirm the presence of atomic carbon and oxygen in the coma and indicate the presence of several species not previously detected in comets. A list of all of the species detected in comet West is given in Table 1. Of particular interest is the presence of carbon in the metastable ^1D state, which cannot be produced in sufficient abundance by direct photodissociation of CO, the most likely immediate parent of the ground state carbon atoms. This suggests a different mechanism for ^1D production and a model based on a CO^+ dissociative recombination source appears to give a satisfactory account of the observations. The details of the model will not be given here but can be found in Appendix A. Since the model does not take into account the plasma diffusion of ions into the tail, it is possible that for comets of low gas production rate the ion densities are too low for recombination to compete with ion diffusion so that the results of the model in such a case would represent an upper limit to the carbon production rate. Photodissociation would then provide a lower limit to the C production rate so that the model, when applied to the mission scenarios should provide a realistic range of estimates of carbon emission brightness and density for mission planning.

Besides carbon, the other strong feature in the spectrum of Fig. 1 is atomic oxygen, which in the case of the comet West observation (heliocentric velocity of 46 km sec^{-1}) is excited by fluorescence induced by solar Lyman β (Feldman et al. 1976). For heliocentric velocity less than $\sim$20 km sec^{-1}, the OI 1304 multiplet is produced by resonance scattering of the solar lines, which would give rise to a λ1304 brightness 10 to 20 times higher than that produced by the Lyman β fluorescence. In fact, a

TABLE 1 Species Observed in Comet West

a.	Observed Species	Strong (*)	Wavelength (Å)
	H I	*	1216
	O I	*	1304
	C I	*	1561, 1657
	C I (^{1}D)		1931
	S I		1814
	C II		1335
	CO		1510
	CS		2580
	OH	*	3090
	CO^+		2200
	CO_2^+		2890
b.	Upper Limits		
	H_2 (CH_4 and H_2CO indirectly)		1608
	CO_2		1993
	NO		2150

measurement of the OI brightness near perihelion, where $\dot{r}$ changes rapidly but r does not, would provide a measure of the solar OI line profiles. In any case, assuming that the C/H_2O ratio to be the same as for comet West, one would expect the oxygen brightness to be comparable to or greater than that for carbon. It is unlikely that any of the other features seen in Fig. 1, and in particular the CO fourth positive bands, would be bright enough in any but the brightest "new" comets to be considered further here. One feature retains some interest, the CII doublet at 1335 Å. The observation of this feature in comet West is not understood since the comet motion ($\dot{r}$) is sufficient to Doppler-shift the solar lines enough to eliminate resonance scattering as an excitation source. It is also not known whether the C^+ ions are an important constituent of the ion tail, even though visible light photographs of comet West made at nearly the same time showed only a dust tail but no ion tail, a feature characteristic of very gassy comets at small heliocentric distances. Thus, it is possible, particularly for a comet with $\dot{r} \lesssim 20$ km sec^{-1}, that the CII 1335 emission could be a very important tracer of one of the principal ion tail constituents.

For the purpose of evaluating the brightness profiles of the dissociation products of H_2O, the formulas of Haser (1957) are used, with modifications to allow for the excess velocity of the products (Festou, 1978). The equations used are summarized in Appendix B. A detailed model calculation by Festou (1978), taking into account the actual velocity distributions of the dissociation fragments as well as the spatial redistribution of the fragment trajectories shows that the Haser formulas give results that are everywhere no more than a factor of two different from the detailed model predictions. This is certainly sufficient for our present aims.

IV. Mission Models and Results

Model calculations are carried out for three different scenarios. The first is the Halley fly-by/Tempel 2 rendez-vous proposed by the Comet Science Working Group, both of which occur at relatively large heliocentric distance ($r \sim 1.5$ a.u.) and which give fairly low ultraviolet surface brightnesses. For comparison, the other two are presumed fly-bys at a value of r close to the comet's perihelion for both Halley and Encke. The gas production rate, and specifically the water production rate, needed for the calculations were taken from models of R. Newburn (1978) based on analyses of visual magnitude as a function of r from previous apparitions of these three comets. The values of Q_{H_2O} used are tabulated in Table 2. In each case, an optimistic assumption is made concerning the relative carbon abundance in choosing a production rate of carbon monoxide, $Q_{CO} = \frac{1}{5} Q_{H_2O}$. This value is derived from analysis of the rocket spectra of comets Kohoutek and West, and the choice of this value for the "old" periodic comets of interest here carries the implicit assumption that the composition of the cometary ice is both homogeneous and the same from comet to comet. This hypothesis remains to be tested and the opportunity to do so may occur with the next apparition of comet Encke in 1980.

The results are presented in graphical form on the following pages in Figures 3 - 9. Each of Figures 3 - 6 consists of five panels showing as a function of ρ, the distance from the center of the nucleus:

a) the density of the ions CO^+, H_2O^+, H_3O^+ and HCO^+, and the total ion density,

b) the density of neutral carbon produced by various sources and the presumed parent CO,

TABLE 2. H_2O Production Rates

	r(au)	Q_{H_2O} (s^{-1}) Pre-perihelion	Q_{H_2O} (s^{-1}) Post-perihelion
Tempel - 2	1.37		6.30×10^{26}
	1.4	1.88×10^{26}	8.65×10^{26}
	1.5	1.13×10^{25}	6.15×10^{26}
	1.6	5.65×10^{24}	4.28×10^{26}
	1.8	---	1.31×10^{26}
Halley	0.6	5.80×10^{29}	5.45×10^{29}
	0.8	1.99×10^{29}	1.76×10^{29}
	1.0	1.12×10^{29}	1.52×10^{29}
	1.2	6.85×10^{28}	1.22×10^{29}
	1.53	3.72×10^{28}	---
	2.0	1.60×10^{28}	4.61×10^{28}
Encke	0.34		4.73×10^{27}
	0.6	3.59×10^{27}	---
	0.8	2.66×10^{27}	---
	1.0	1.74×10^{27}	---
	1.5	3.35×10^{26}	---

c) the brightness of the CI λ1657 and CO (1,0) fourth positive emissions,

d) the densities of the water dissociation products, H and OH,

e) the brightness of the HI Lyman α line and the OH (0,0) band near 3090 Å.

The four cases presented here are for comet Halley at 1.53 a.u. and 0.6 a.u., comet Tempel 2 at 1.37 a.u. (perihelion) and comet Encke at 0.34 a.u. (perihelion).

As noted above, a principal source of carbon emission is the dissociative recombination of CO^+ ions as evidenced by the large abundance of $C(^1D)$ detected in comet West. However, comet West was a particularly gassy comet and hence the densities in the coma may have been particularly favorable for recombination to be the main loss mechanism for CO^+ ions. This appears to be borne out by the absence of a visible ion tail in photographs of the comet taken on the same day that the ultraviolet observations were made. As the densities decrease, the importance of recombination may decrease relative to plasma diffusion of CO^+ ions into the tail with a consequent reduction in the contribution of this source to the total C atom production. In the worst case, that of very low densities, carbon would be produced by photodissociation of its parent (CO) alone. The actual case probably lies somewhere inbetween the two extreme cases of high density, no ion tail and low density, no recombination, but since there is no way to provide a reliable estimate, the extreme range of values of the CI λ1657 brightness is indicated by cross-hatching in (c) of Figures 3 - 6.

At large heliocentric distances, the carbon parent, CO, survives to large distances from the nucleus, so that the brightness of the CO (1,0) fourth positive band at 1510 Å will be brighter than the CI 1657

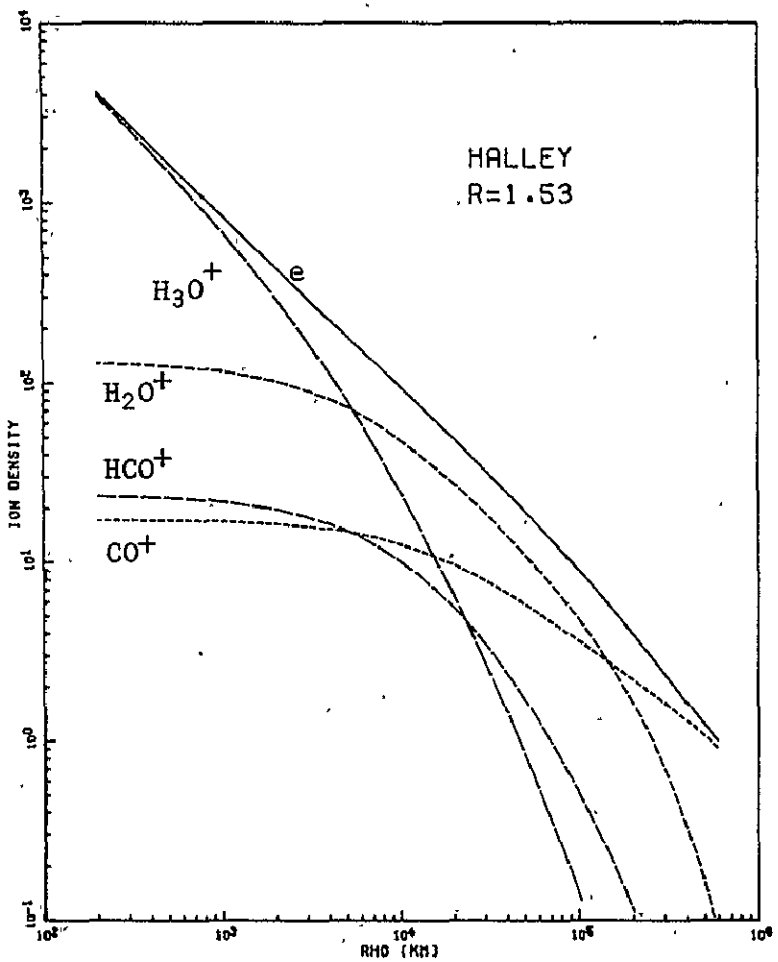

Figure 3a. Electron and ion densities derived from model. Comet Halley, r=1.53 au.

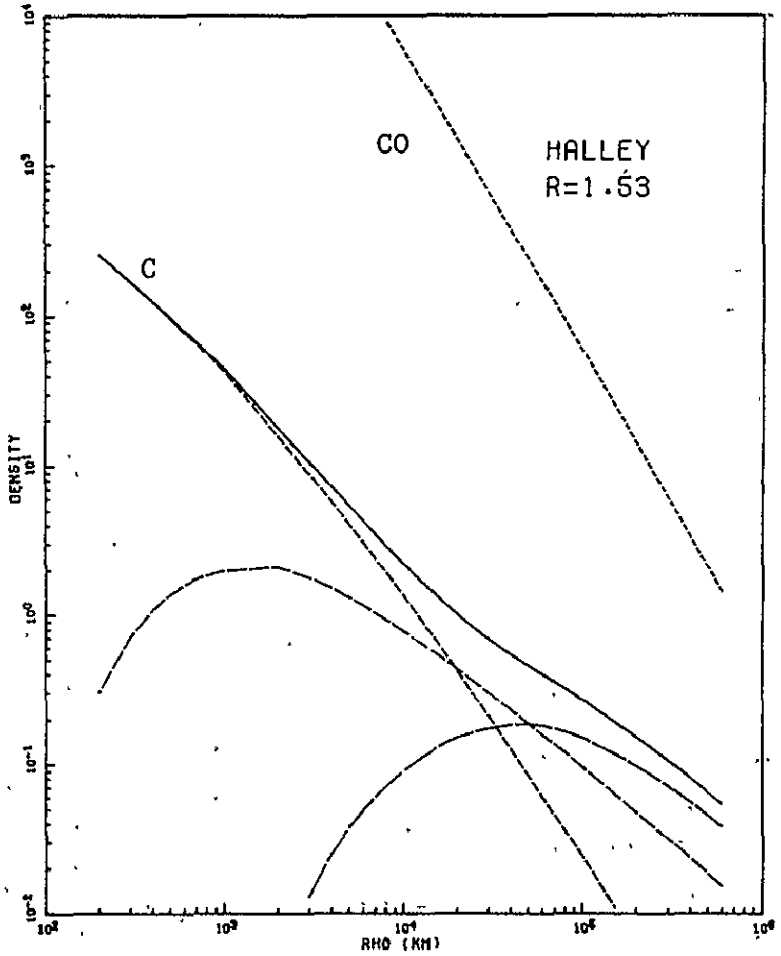

Figure 3b. C and CO densities derived from model. The C density is the sum of three different components (see Appendix A). Comet Halley, r=1.53 au.

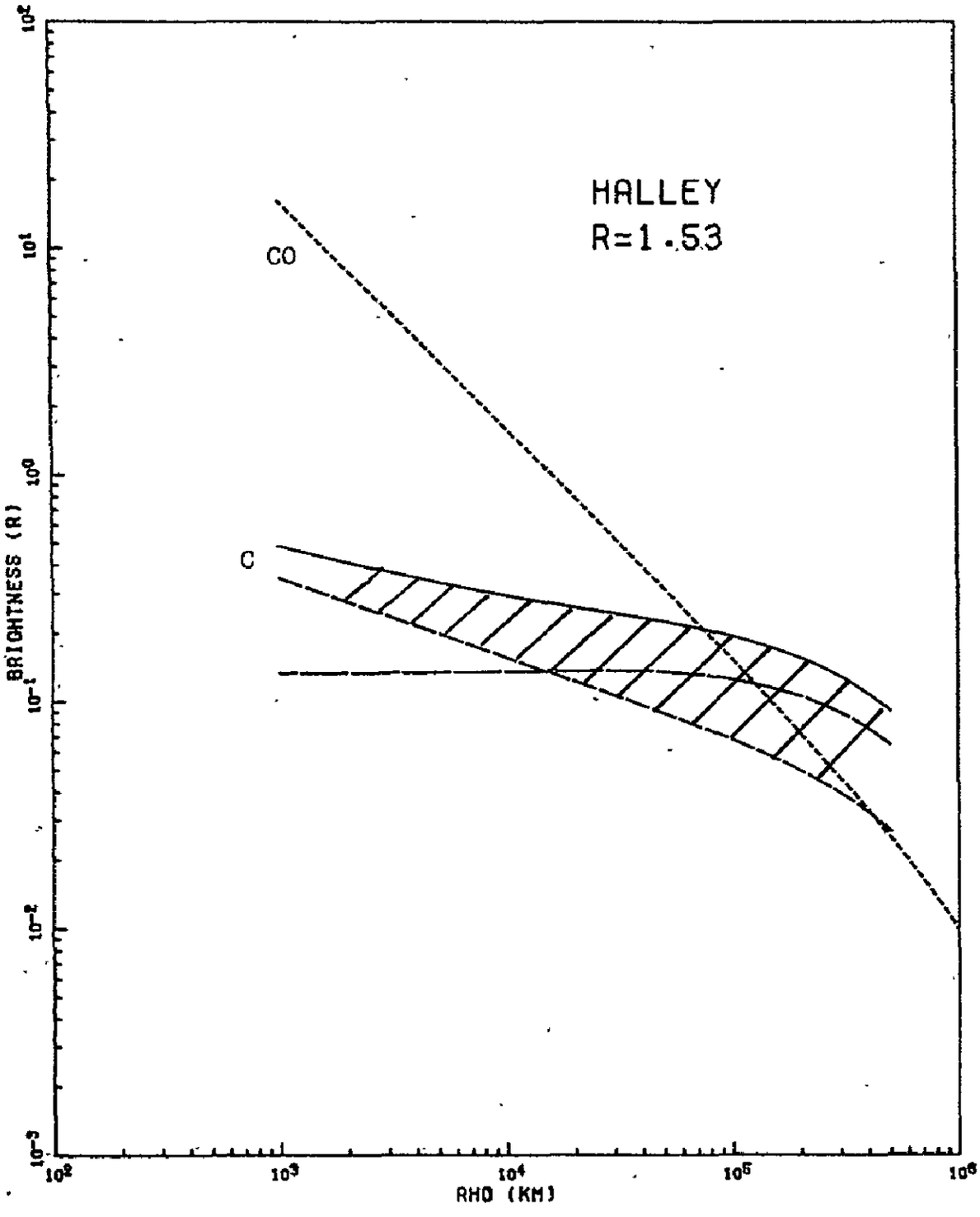

Figure 3c. Brightness of the CI 1657 line and the CO (1,0) fourth positive band at 1510 Å derived from the model. The cross-hatching indicates the range of possible values for the carbon line. Comet Halley, r=1.53 au.

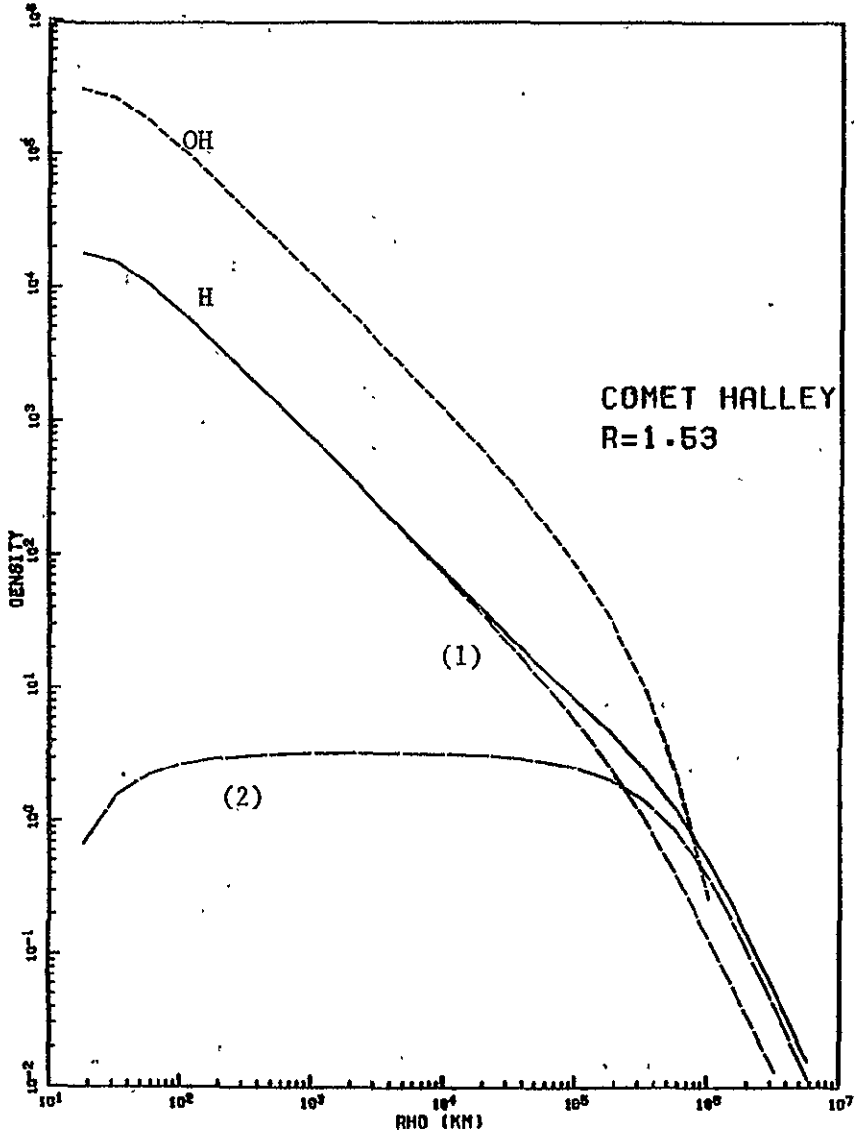

Figure 3d. H and OH densities resulting from photo-dissociation of H_2O. The curves marked (1) and (2) represent H produced by dissociation of H_2O and OH, respectively. Comet Halley, r=1.53 au.

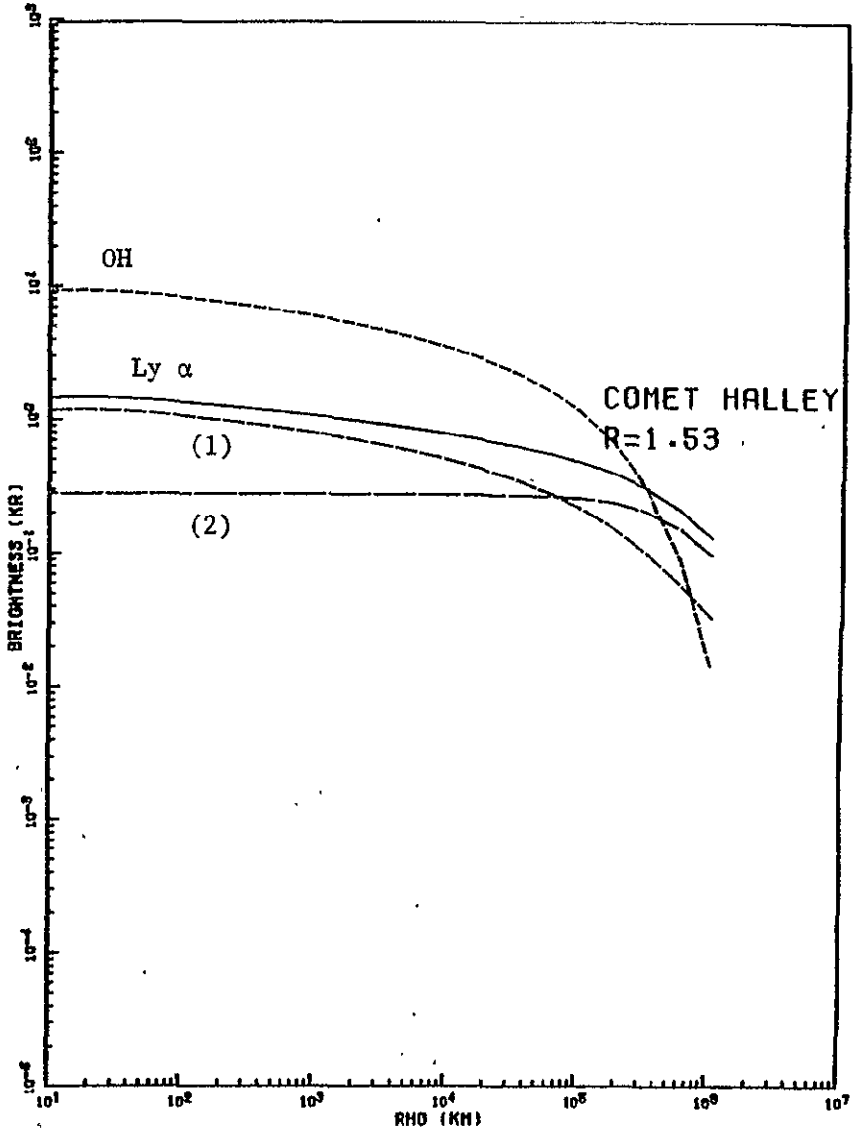

Figure 3e. Brightness of the OH (0,0) 3090 Å band and HI Lyman α. The curves marked (1) and (2) have the same significance as in Fig. 3d. Comet Halley, r=1.53 au.

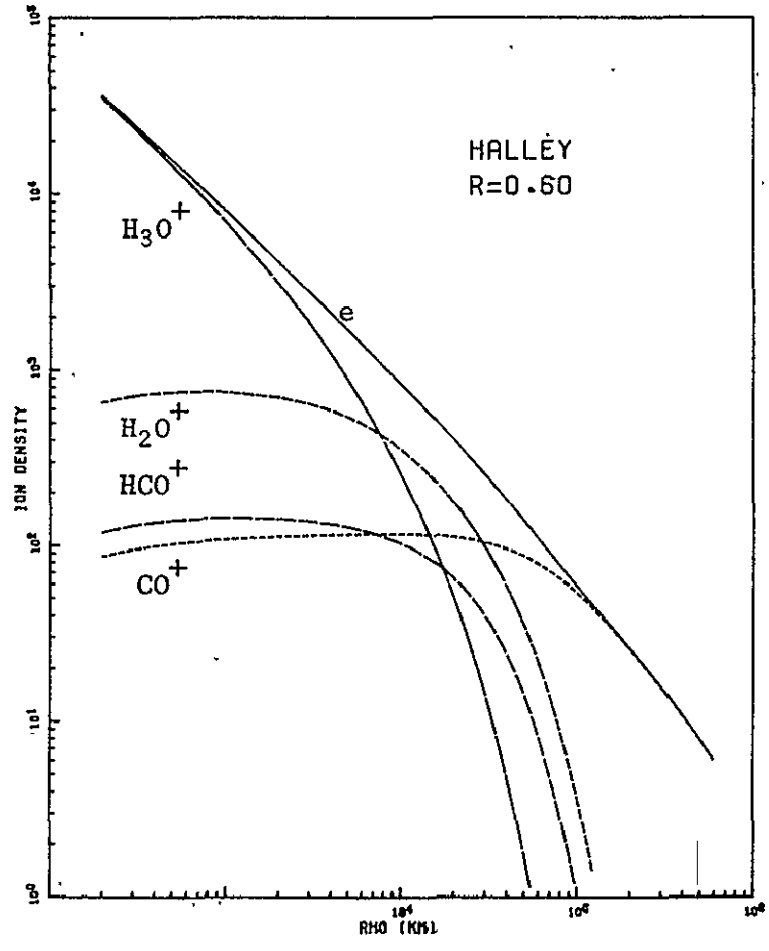

Figure 4a. Same as Fig. 3a, Comet Halley, r=0.6 au.

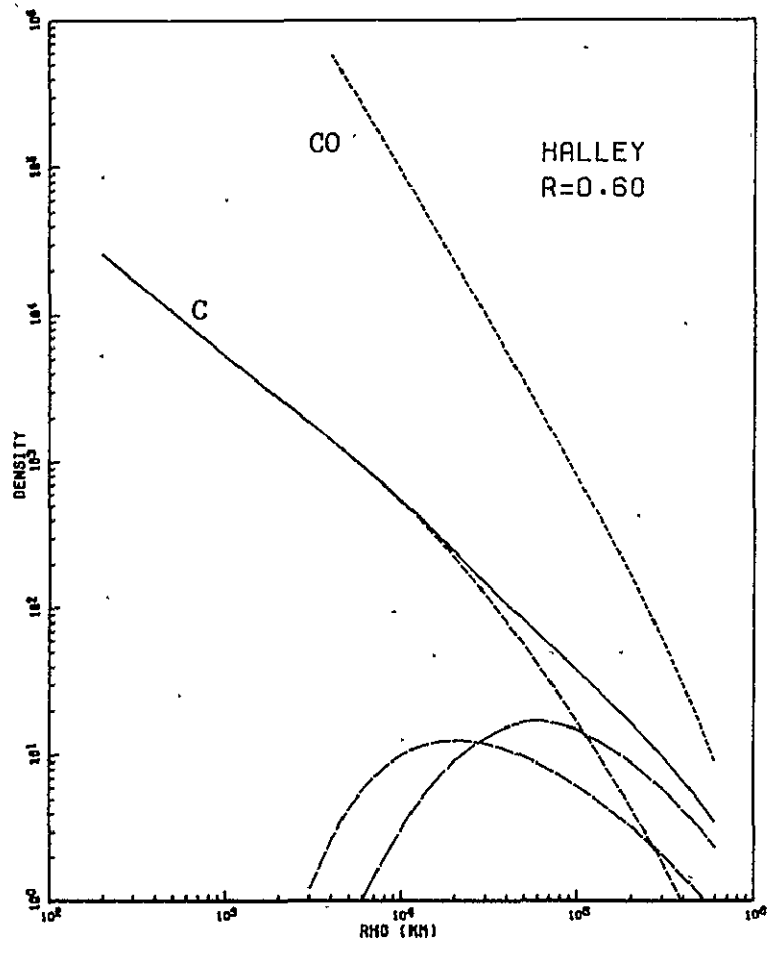

Figure 4b. Same as Fig. 3b, Comet Halley, r-0.6 au.

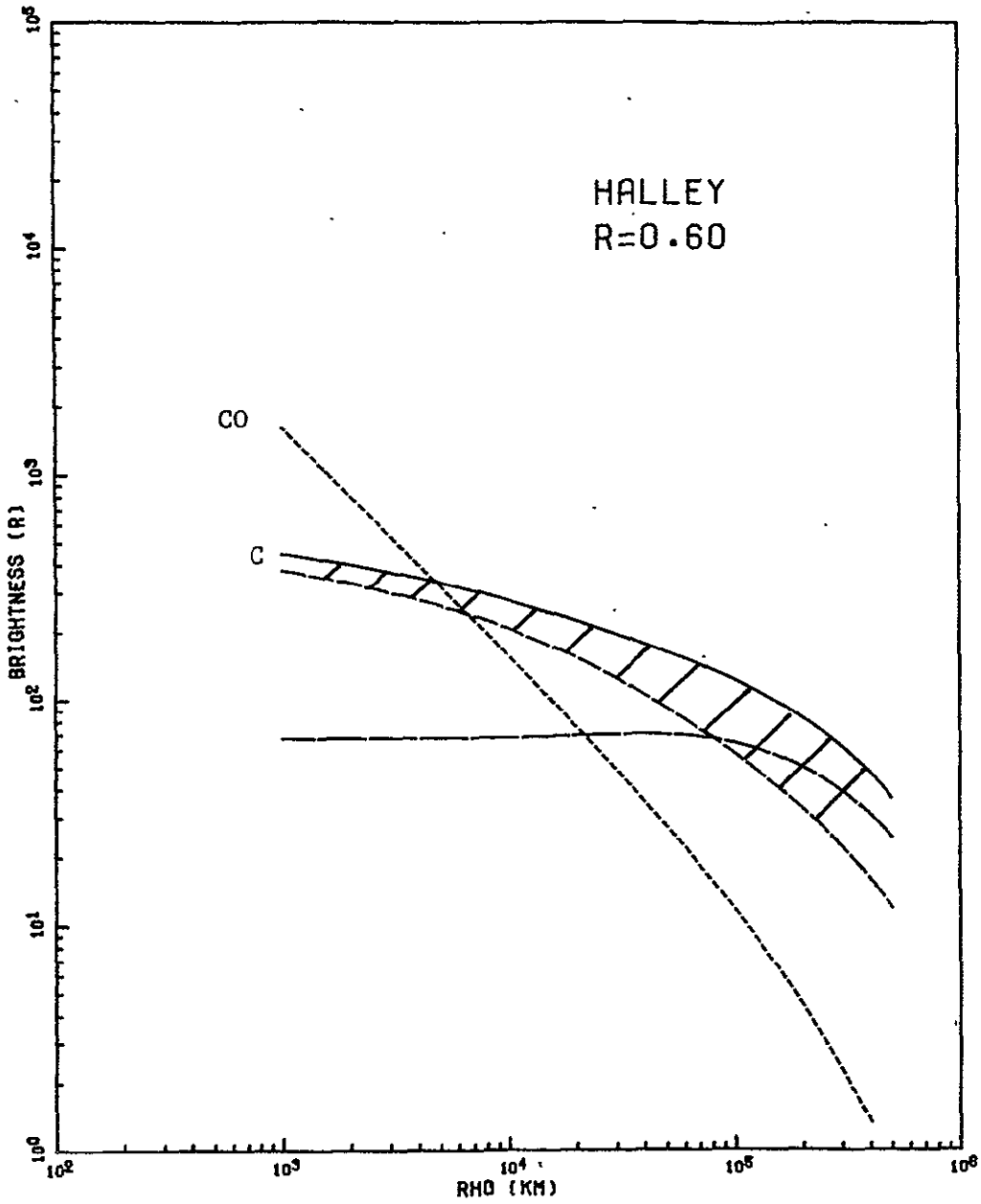

Figure 4c. Same as Fig. 3c, Comet Halley, r=0.6 au.

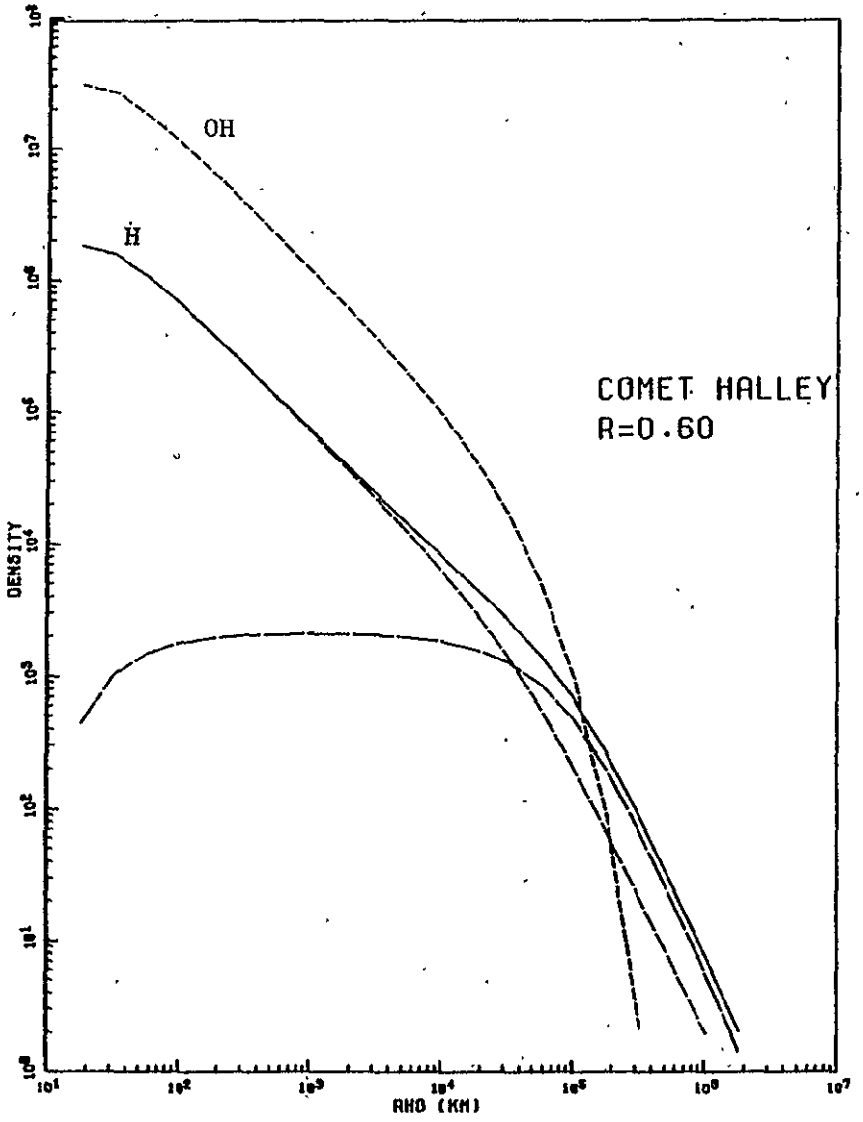

Figure 4d. Same as Fig. 3d, Comet Halley, r=0.6 au.

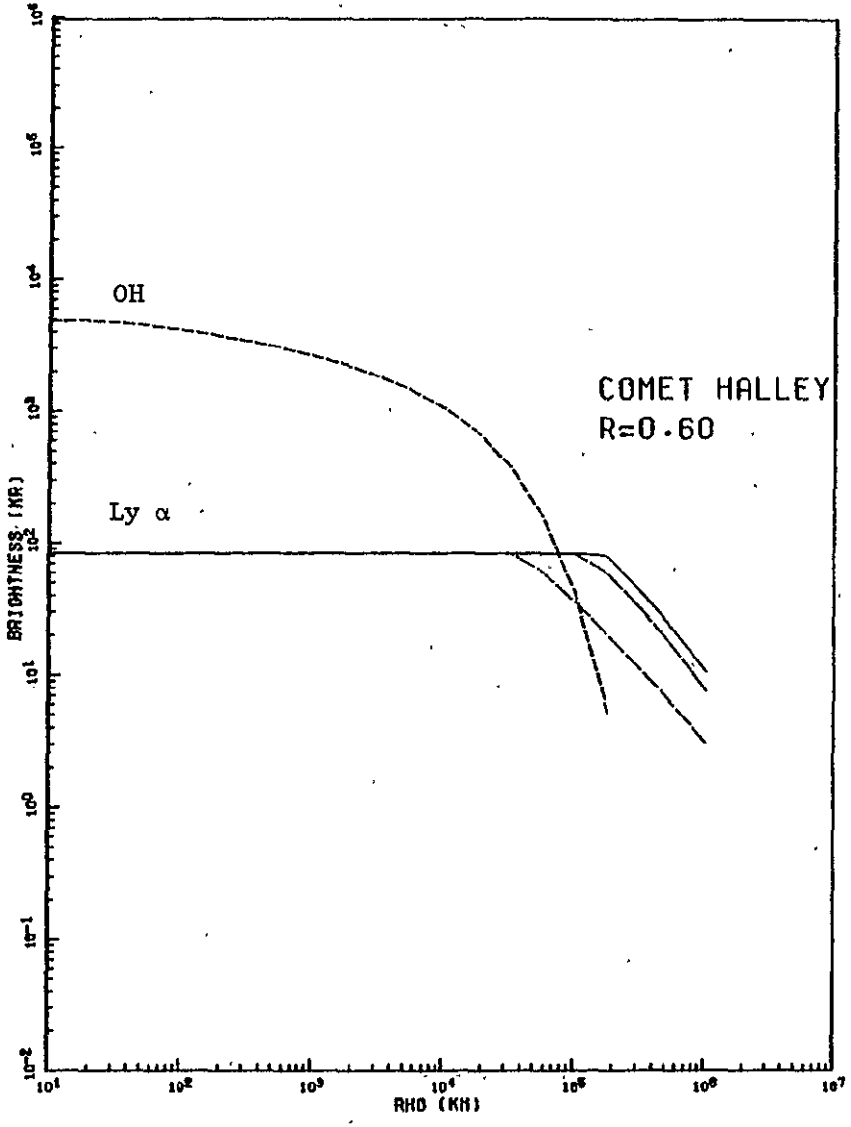

Figure 4e. Same as Fig. 3e, Comet Halley, r=0.6 au. Note that HI Lyman α is optically thick in this case.

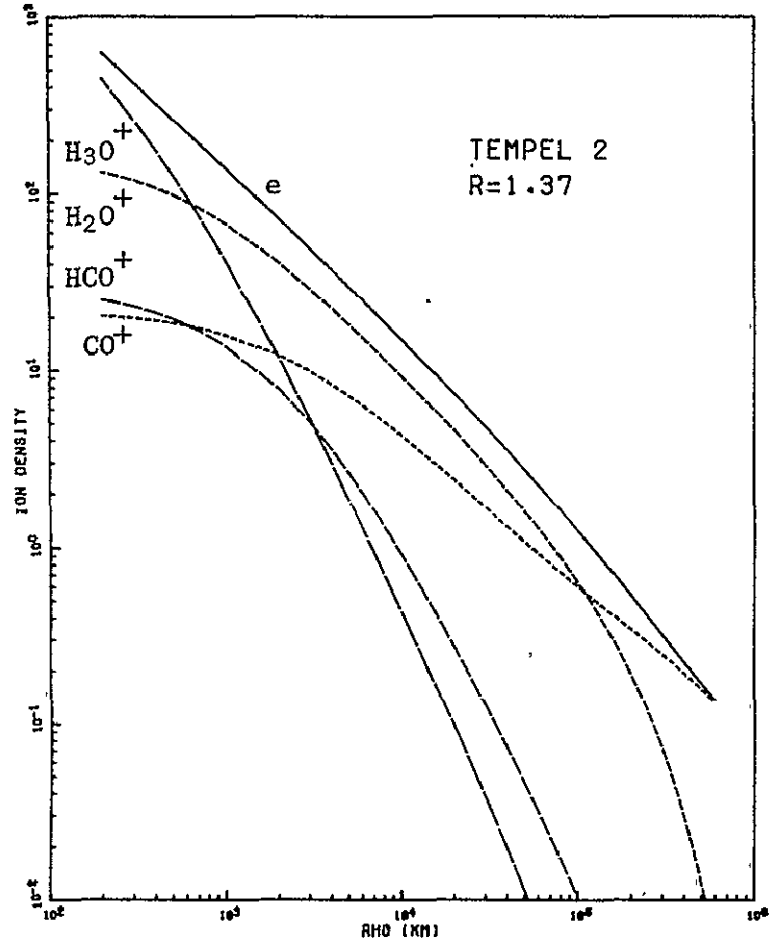

Figure 5a. Same as Fig. 3a, Comet Tempel 2, perihelion.

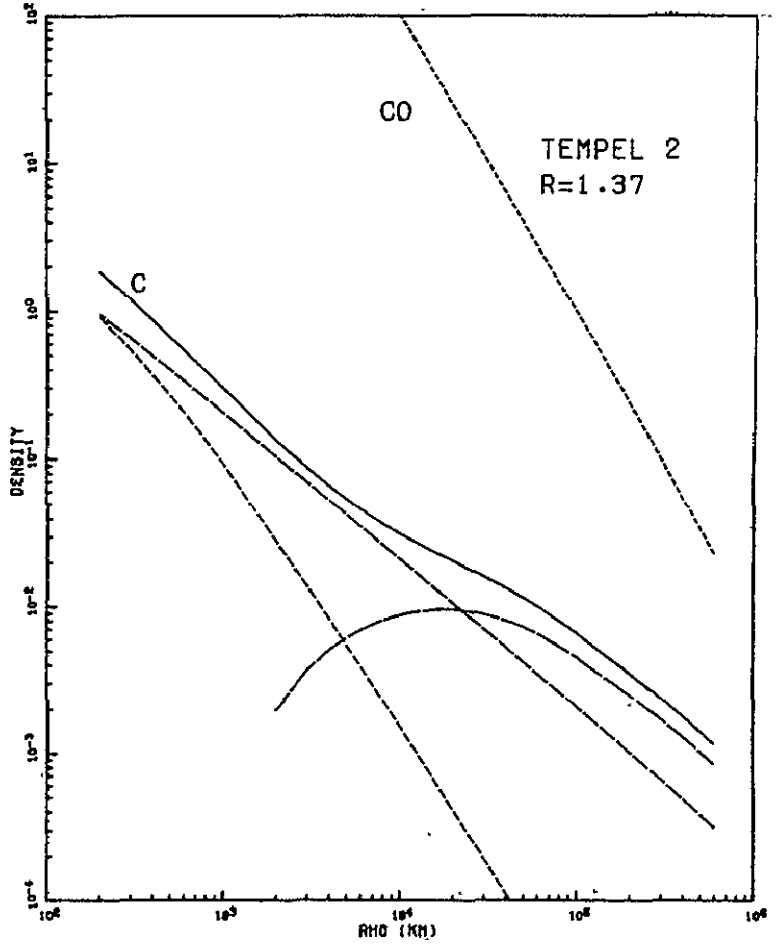

Figure 5b. Same as Fig. 3b, Comet Tempel 2, perihelion.

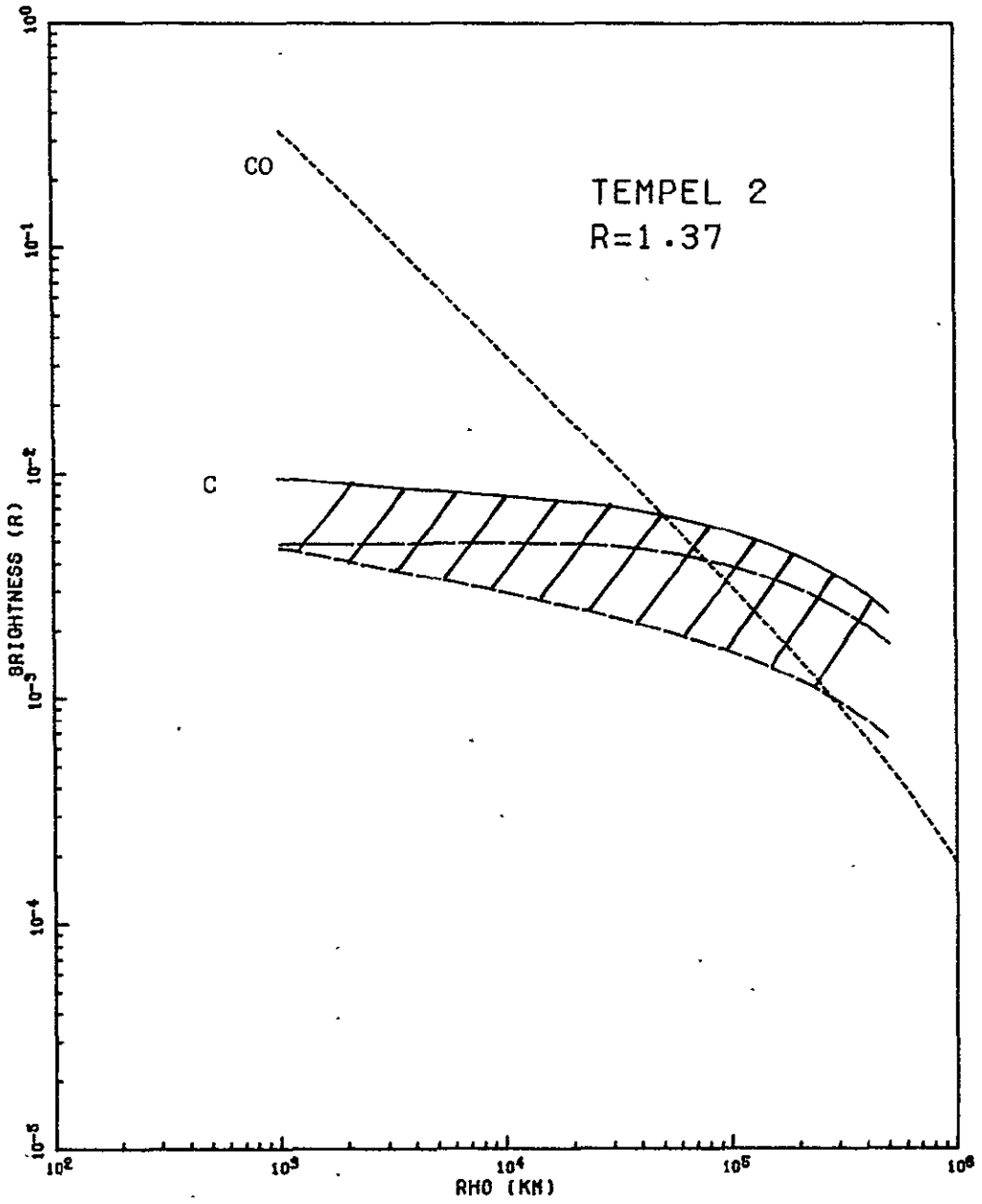

Figure 5c. Same as Fig. 3c, Comet Tempel 2, perihelion

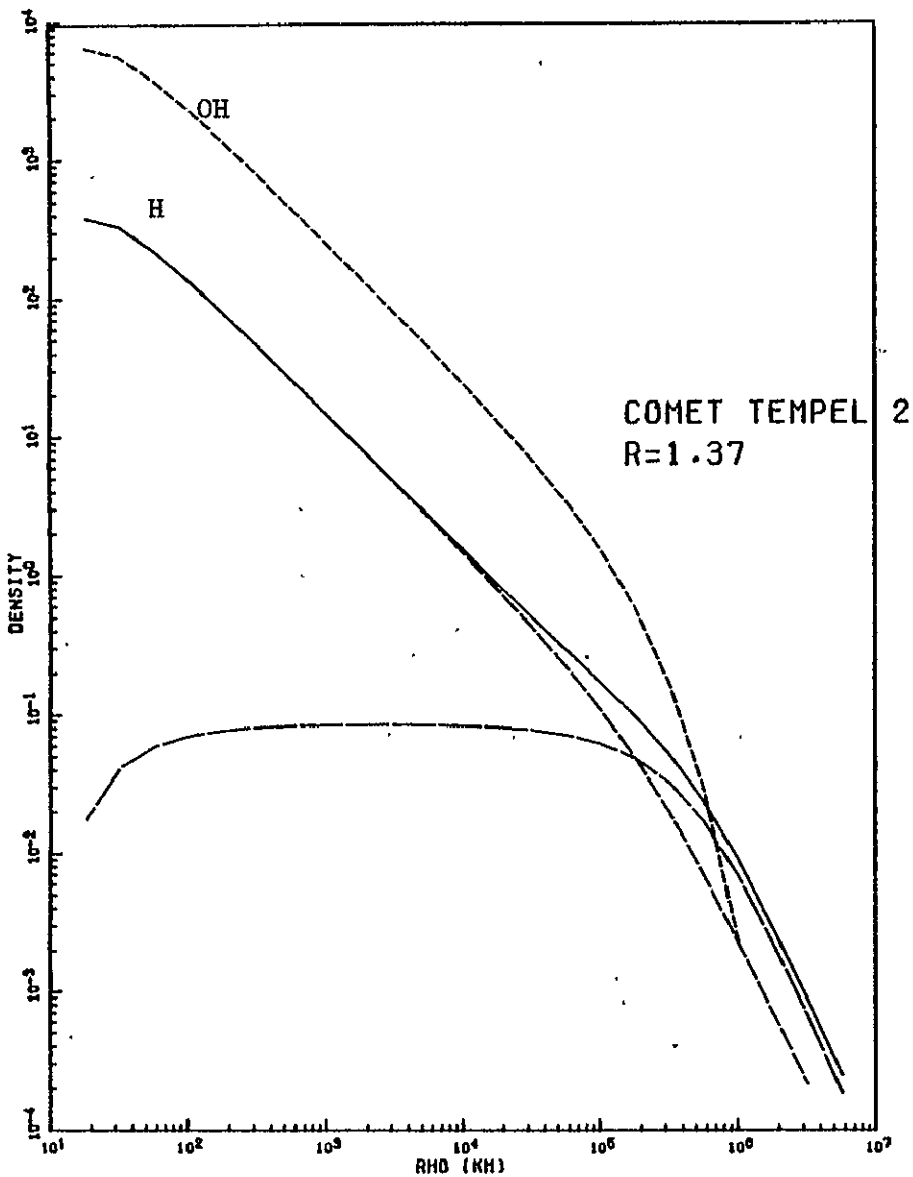

Figure 5d. Same as Fig. 3d, Comet Tempel 2, perihelion.

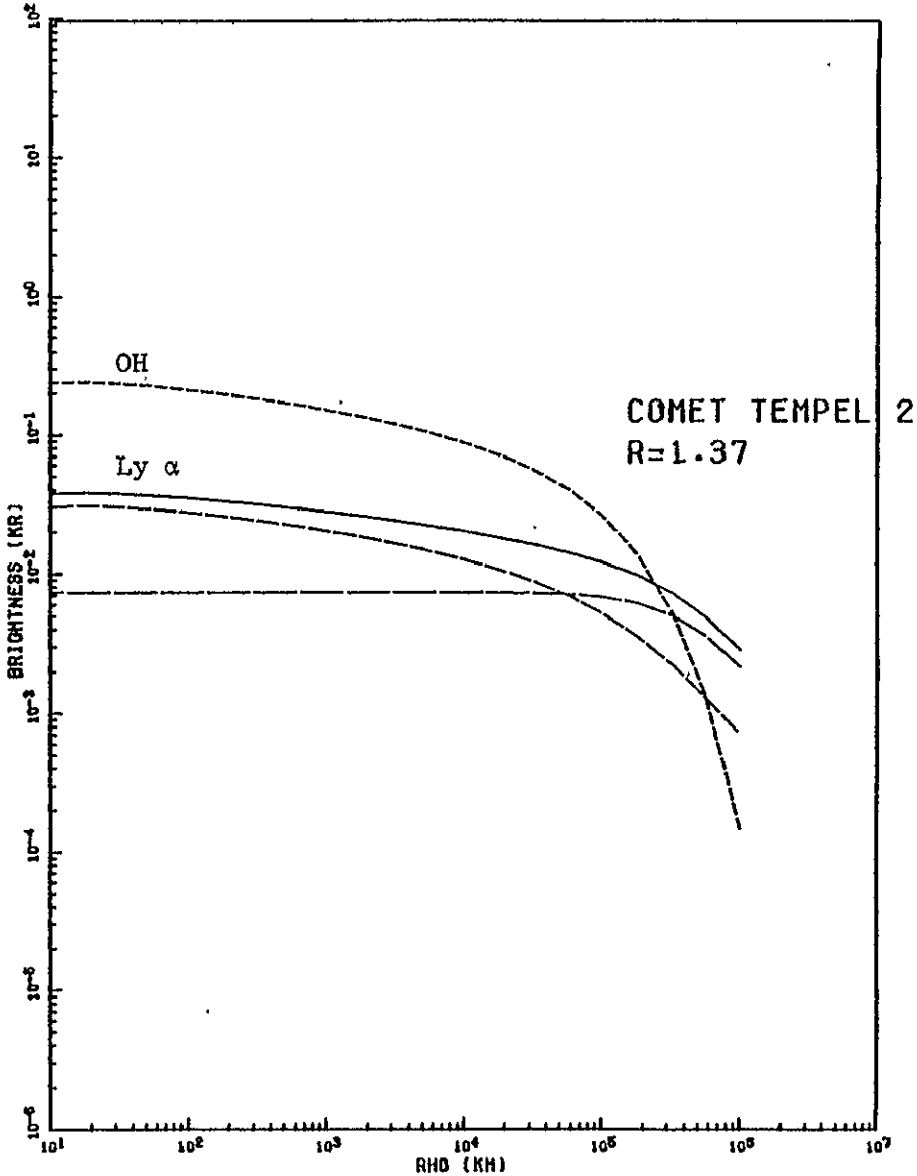

Figure 5e. Same as Fig. 3e, Comet Tempel 2, perihelion.

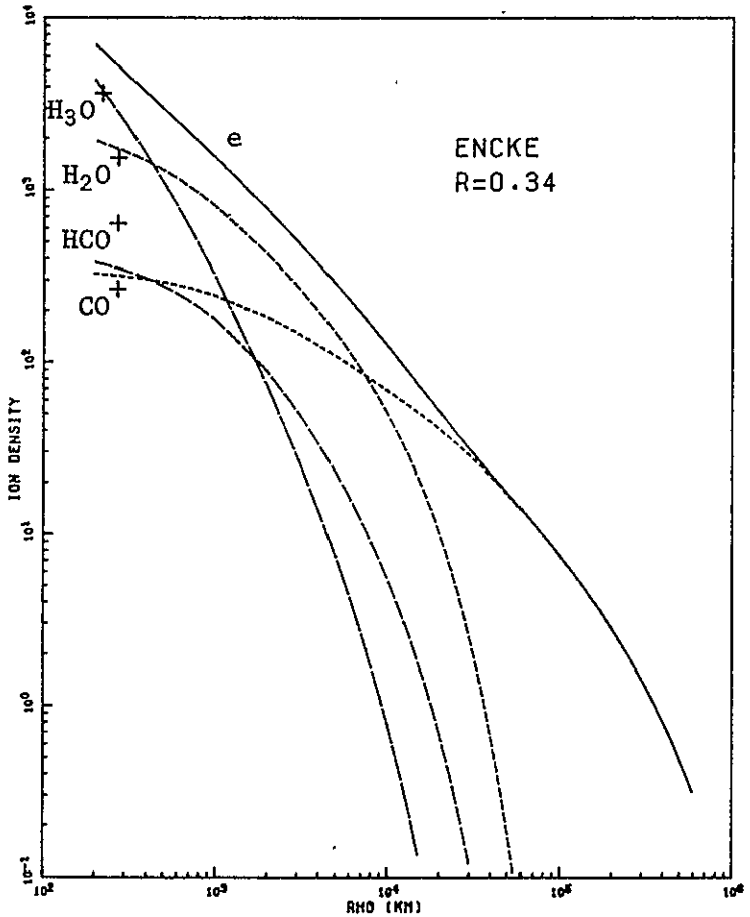

Figure 6a. Same as Fig. 3a, Comet Encke, perihelion

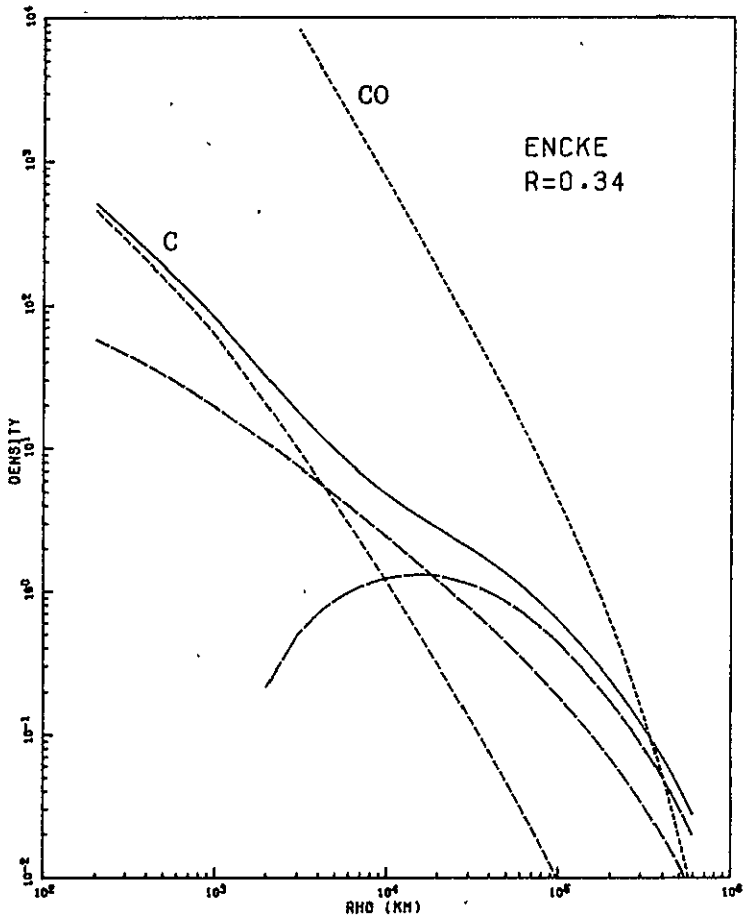

Figure 6b. Same as Fig. 3b, Comet Encke, perihelion.

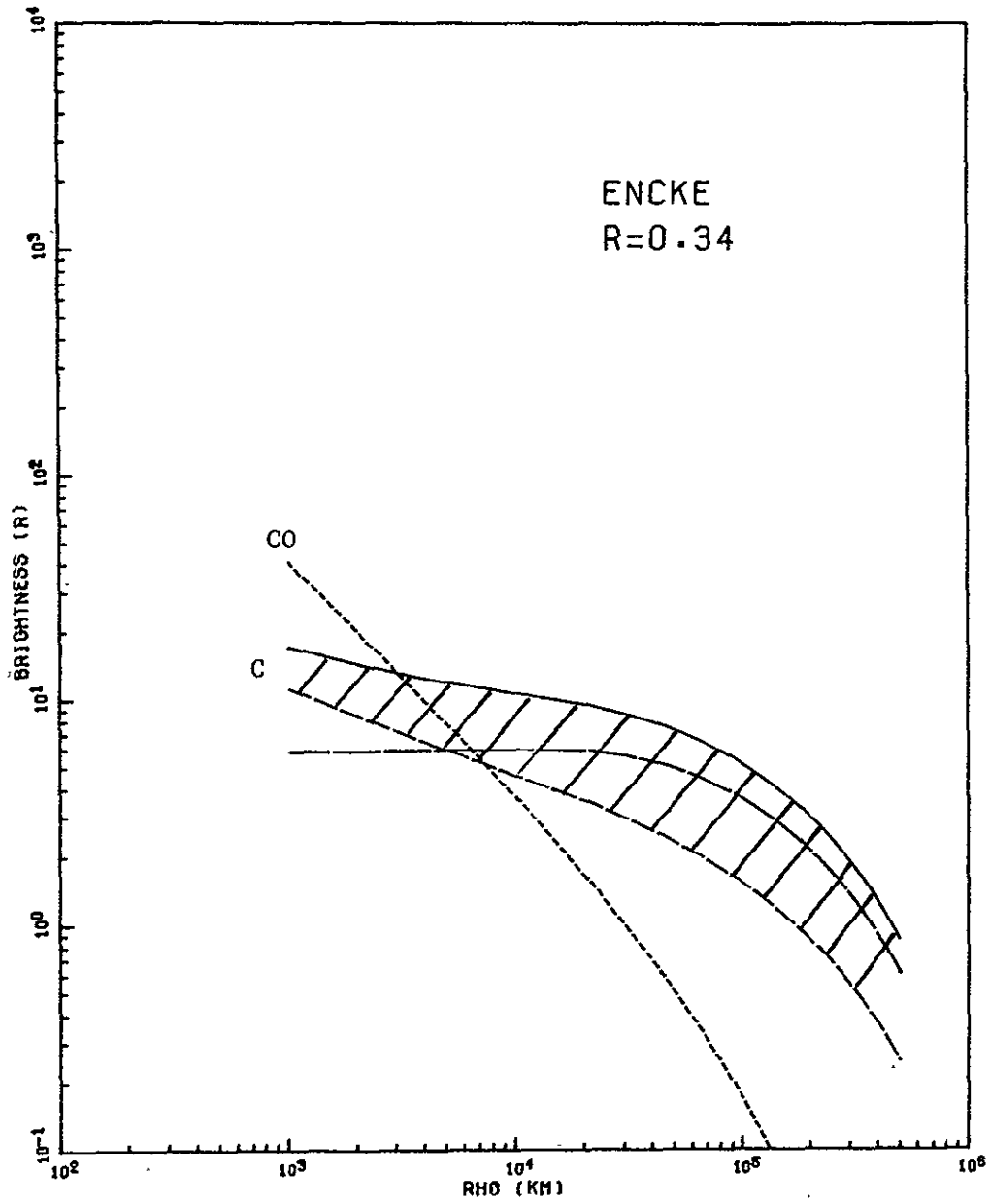

Figure 6c. Same as Fig. 3c, Comet Encke, perihelion.

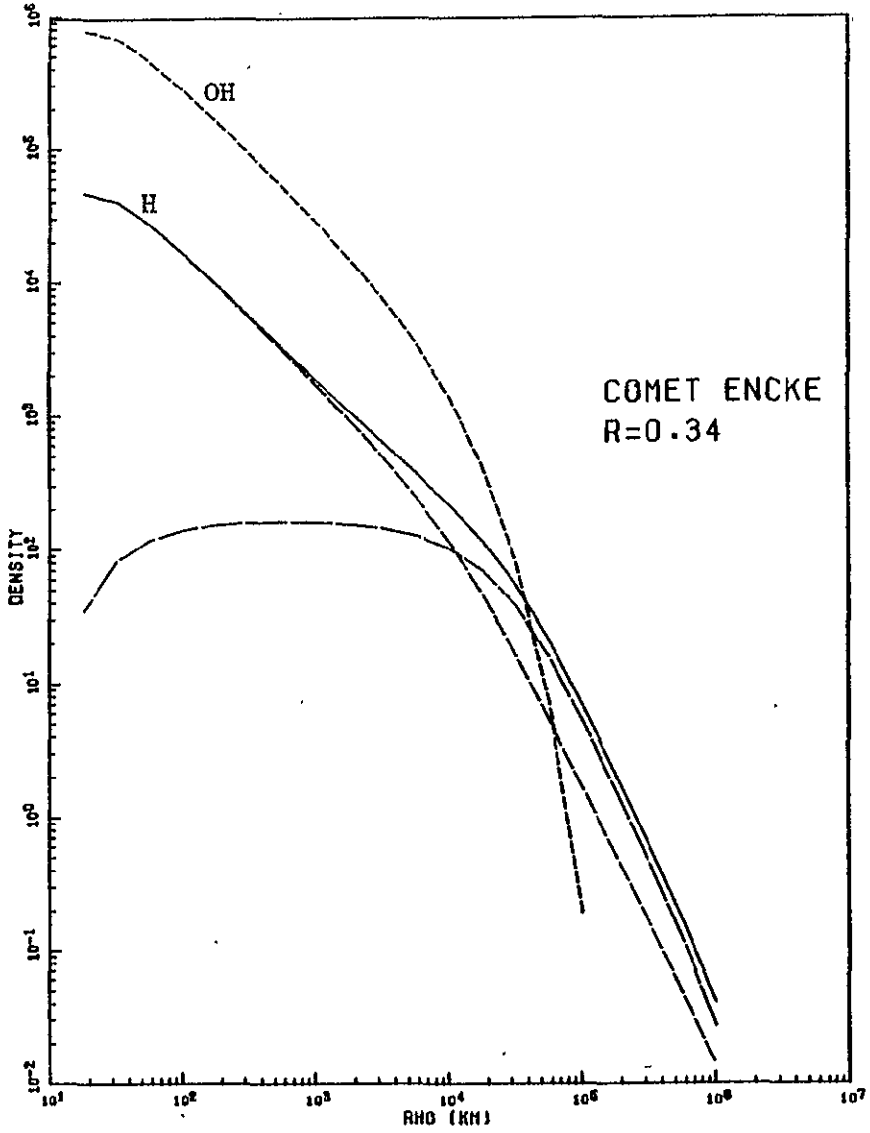

Figure 6d. Same as Fig. 3d, Comet Encke, perihelion

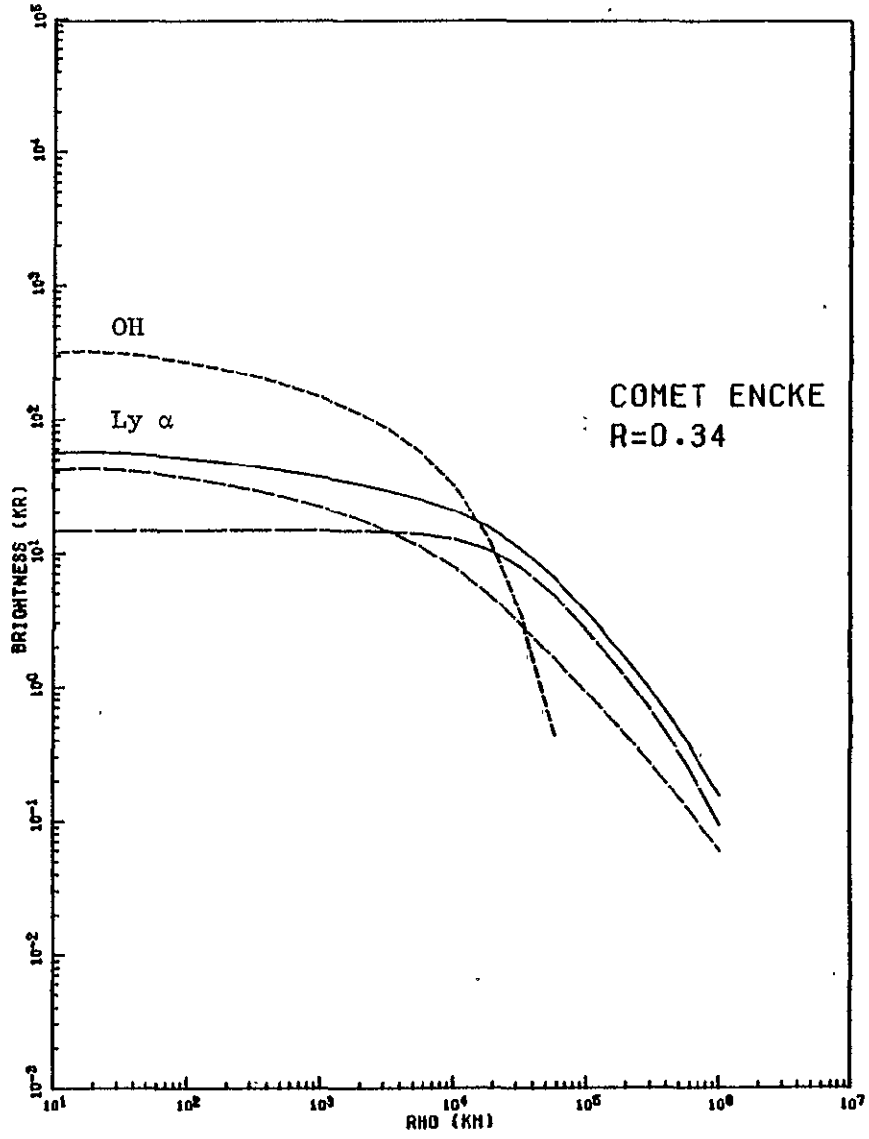

Figure 6e. Same as Fig. 3e, Comet Encke, perihelion.

line. This is in marked contrast to the situation at small heliocentric distance as evidenced by the Comet West data (r = 0.385 a.u.) shown in Fig. 1 and can be clearly seen in a comparison of Figs. 3c and 4c. Thus, it appears that for the conditions of the Halley/Tempel 2 mission the CO emission may be more easily detectable than that from atomic carbon.

The strong dependence of the ultraviolet emission on heliocentric distance r is illustrated in Figures 7 - 9 which gives the CI 1657 brightness for comets Halley, Tempel 2 and Encke. The dependence of the brightness on r is roughly $\sim r^{-6}$ for a gas production rate that varies as r^{-2}. If the entire ultraviolet coma (in this case carbon) is observed, the observed flux will vary as $\sim r^{-2}$, but the projected size of the emitting volume will increase by a factor r^2, or r^4 in area. To obtain information about the basic ion chemistry of the coma, it is necessary to measure the brightness, B, of the different emission features as a function of the distance from the nucleus ρ, and in order to achieve sufficient spatial resolution, an angular field-of-view much smaller than the angular extent of the coma must be used. Consequently, this measurement is severely limited by the strong variation in B with heliocentric distance and the choice of a fly-by and rendezvous near 1.5 a.u. is not a particularly happy one from the viewpoint of ultraviolet spectroscopy.

A measurement of the total flux at a given wavelength provides a direct determination of the total production rate of the particular species (Feldman and Brune 1976) but care must be taken to ensure that radiation from the entire coma is collected. In this case, however, the variation in total flux varies with r as the gas production rate, typically as r^{-2}, so that instrument sensitivity is not as serious a consideration as it is for brightness measurements. Such a mode of observation, though, is

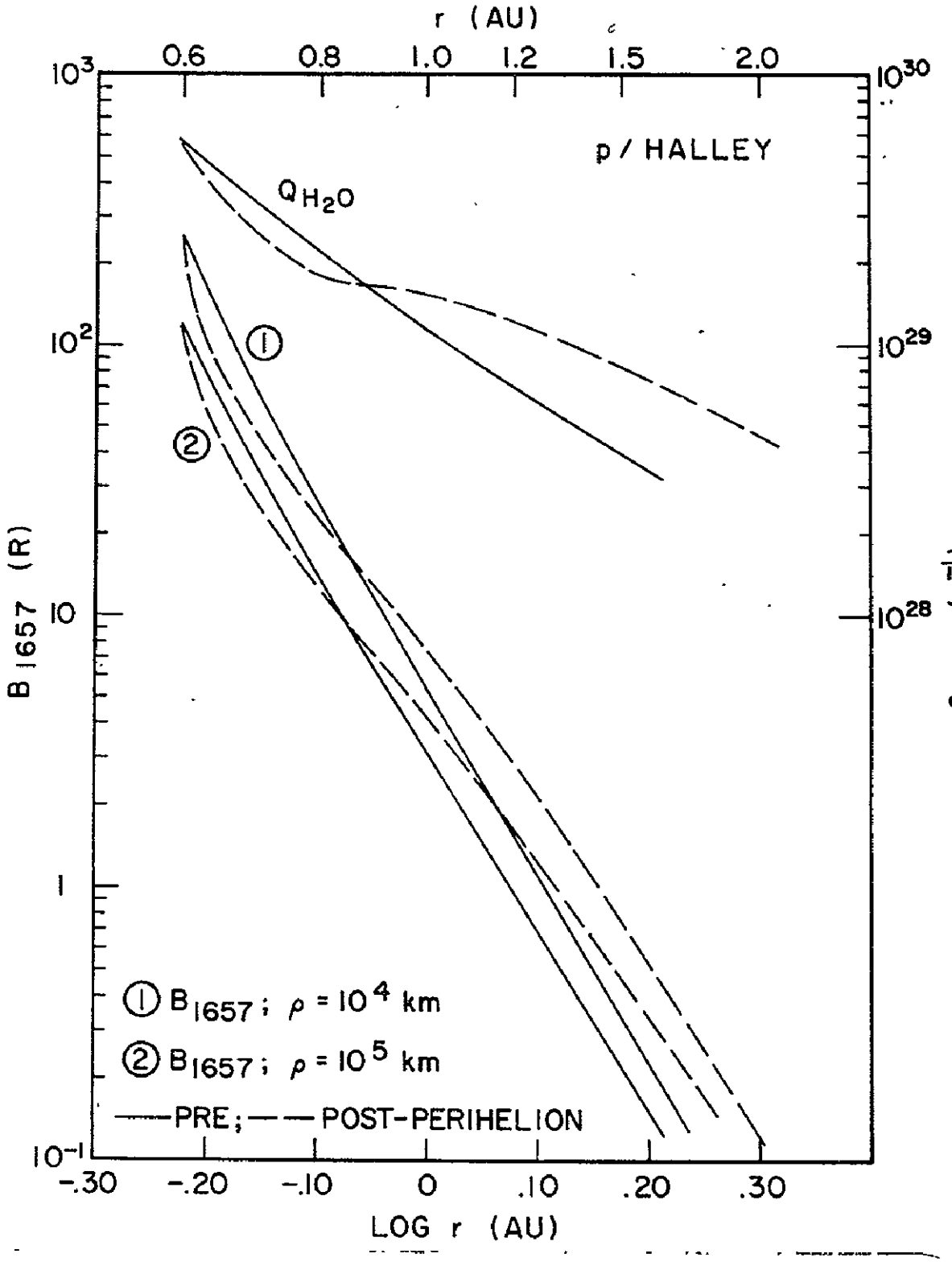

Figure 7. Variation in CI 1657 brightness as a function of heliocentric distance. Comet Halley

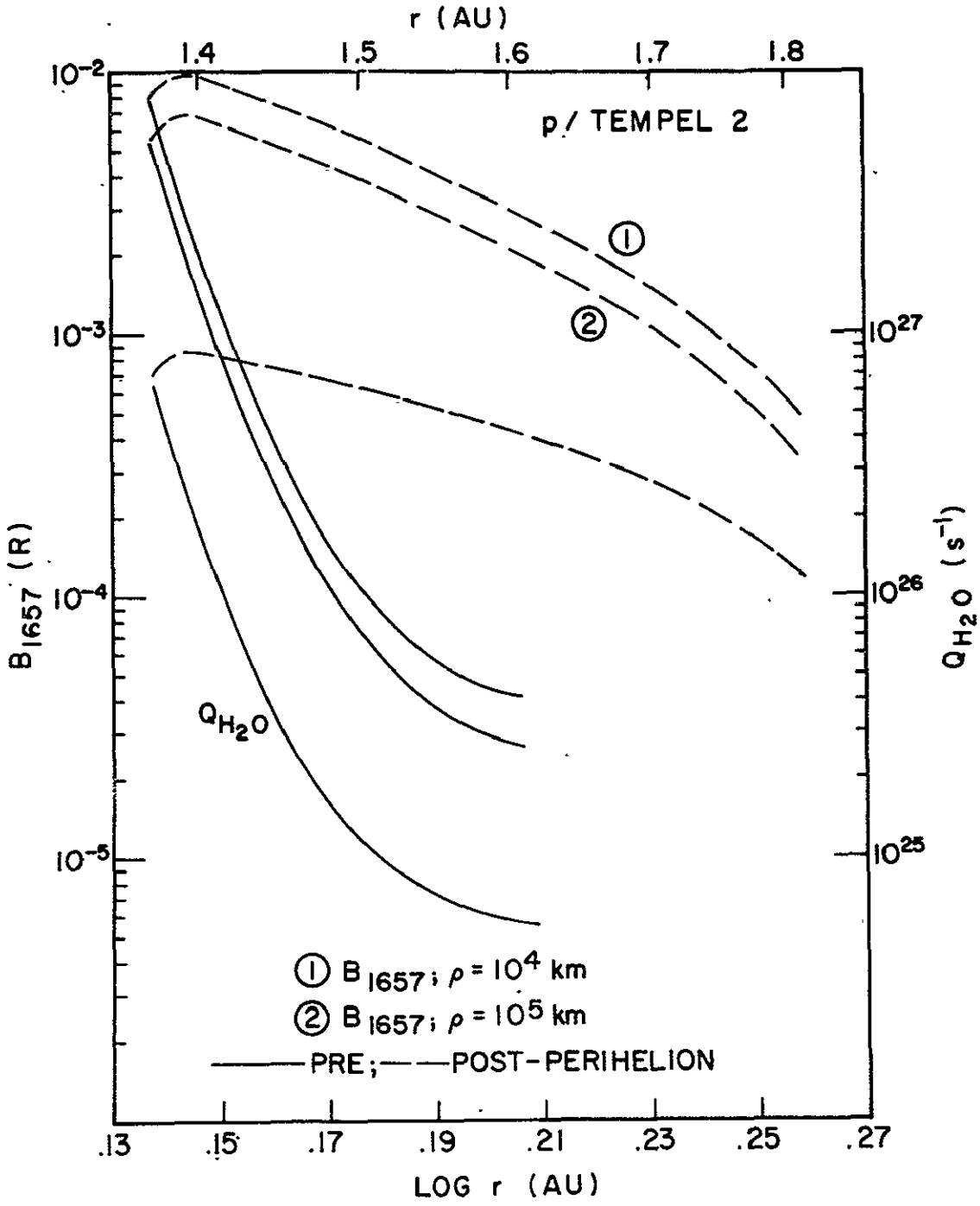

Figure 8. Same as Fig. 7, Comet Tempel 2.

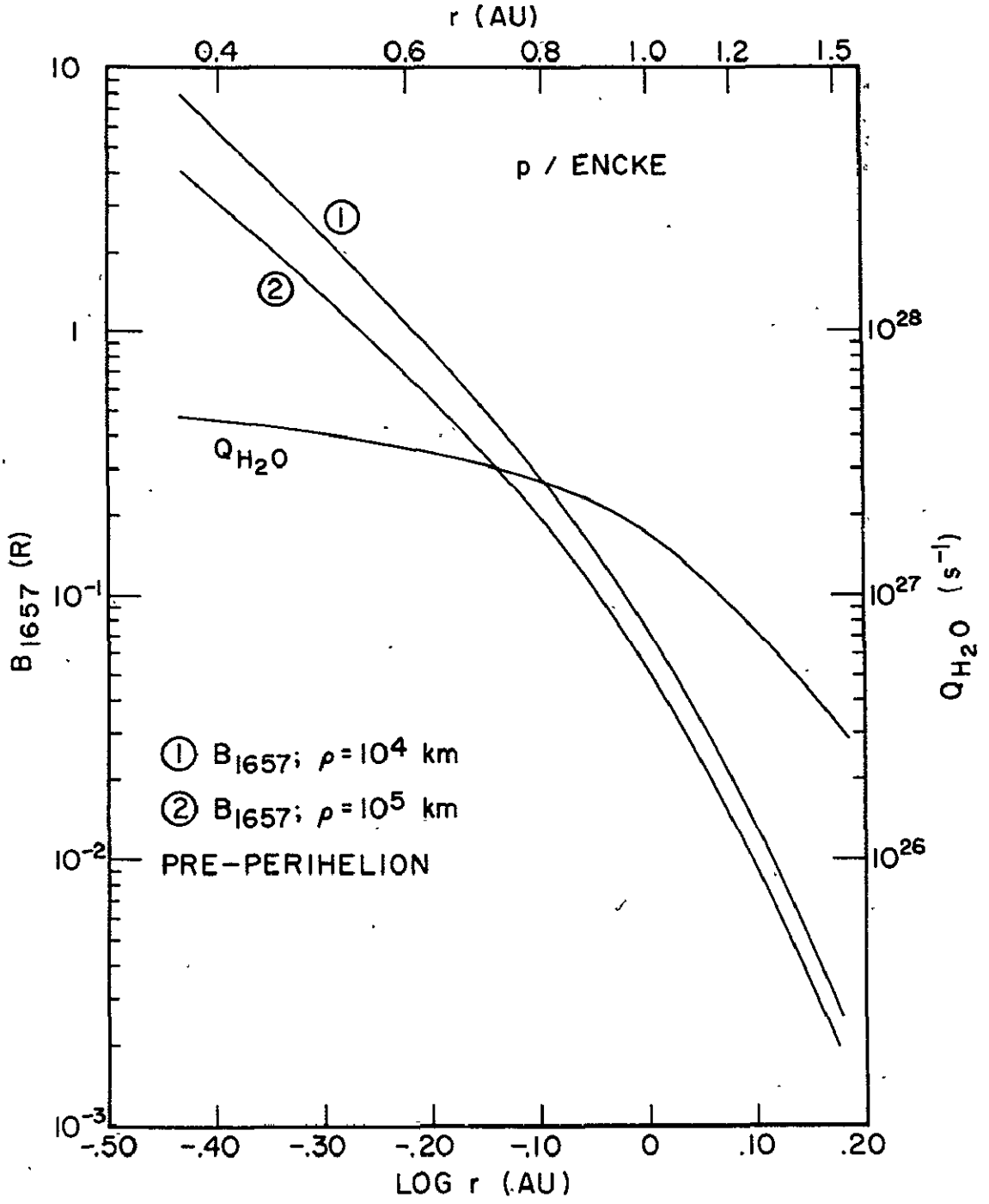

Figure 9. Same as Fig. 7, Comet Encke, pre-perihelion only.

impractical for a fly-by (and particularly for a rendez-vous) as the angular size of the coma changes quite rapidly and becomes very large near encounter.

The model results for the Halley fly-by/Tempel 2 rendez-vous mission are summarized in Table 3. The densities of the principal neutral species and the total ion density are given at $\rho = 10^5$km for Halley and at $\rho = 100$ and 1000 km for Tempel 2. The ultraviolet brightnesses are given for Halley looking both outward and inward, while for Tempel 2 only outward viewing is considered. Bearing in mind that these results are derived from a rather rudimentary model based on a limited amount of observation, the conclusions to be drawn are the following:

a. The only ultraviolet emission features that can be observed, with the present state-of-the-art in ultraviolet spectroscopic instrumentation, during a Halley fly-by/Tempel 2 rendez-vous mission would be HI Ly α and the OH (0,0) band at 3090 Å. The CI 1657 multiplet, which is the next strongest feature (excluding other OH bands and CO^+ or CO_2^+ also observable in the blue or near-ultraviolet) in the spectrum of "new" comets (Feldman and Brune 1976), is less than 1 Rayleigh in both cases and would require instrumentation of large volume and weight for observation.

b. The observation of HI Ly α in comet Tempel 2 will be extremely marginal due to the background of solar Ly α resonantly scattered from interplanetary hydrogen atoms which is typically $\sim$300 R (the actual value depends on the relative orientation between the viewing direction and the apex of the interstellar wind) or about 10 times larger than the expected cometary Ly α brightness.

TABLE 3. Model Results for Halley Fly-by/Tempel 2 Rendezvous mission.

	Halley r = 1.53 a.u.	Tempel 2 r = 1.37 a.u.	
Densities (cm^{-3})	$\rho = 10^5$km	$\rho = 10^2$km	$\rho = 10^3$km
H_2O	160	4.8×10^6	4.8×10^4
CO	60	1.0×10^6	1.0×10^4
OH	80	2,300	250
H	8	135	15
C	0.25	4	0.3
Total ion	9	1,200	140
Surface Brightness (R)			
Ly α (looking out)	240	17	14
(looking in)	480	--	--
OH (looking out)	600	150	75
(looking in)	4,000	--	--
CI 1657 (looking out)	0.10	0.005	0.005
(looking in)	~0.5	--	--
CO (1,0) (looking out)	0.10	1.7	0.2
(looking in)	~5	--	--

c. A similar but much less severe background problem exists at 3090 Å, the mean wavelength of the OH (0,0) band, in the form of zodiacal light which is of the order of 0.5 R/A at 90^{o} elongation. This problem could be important, in the case of Tempel 2 only, if a broad-band photometer were to be used to monitor this emission as a measure of the H_2O production rate.

In summary, it appears that an ultraviolet spectrometer is not a good candidate instrument for a Halley fly-by/Tempel 2 rendez-vous mission. This is not meant to exclude the possibility of using small, compact, narrow-band photometers at HI Ly α and OH λ3090 as a means of determining the water vaporization rate from the nucleus as well as to determine the response of this production rate to variations in solar activity. It is also suggested that the specifications of any proposed neutral or ion mass spectrometer be closely examined in the light of the densities given in Table 3. By contrast an examination of Figs. 4, 6, 7 and 9, shows that a mission involving a fly-by of either Halley or Encke near perihelion would be an excellent candidate from the point of view of ultraviolet spectroscopy.

V. Application to Space Telescope Observations

In this section we briefly consider the suggestion that Space Telescope (ST) be used to provide support in the form of ultraviolet observations during the two encounters of the Halley/Tempel 2 mission. The applicable ST focal plane instrument is the Faint Object Spectrograph (FOS). Relevant parameters of the FOS were obtained from A. F. Davidsen of Johns Hopkins University, who is a member of the FOS team. Since ST will be in Earth orbit, HI Ly α observations of both comets will be further hampered by the strong geocoronal Ly α emission whose minimum value (at local midnight) is 1.5 - 2.0 kR during solar minimum. In principle, at sufficiently high resolution the cometary Ly α, which is Doppler shifted relative to the Earth (0.04 $\mathring{A}$ = 10 km sec^{-1}) can be spectrally separated from the geocoronal line, but in the case of Halley, the fly-by occurs at minimum Earth-comet distance (0.6 a.u.) where the Doppler shift is zero.

For a source of brightness B in Rayleighs, the observed count rate S is given by

$$S = B \cdot \frac{10^6}{4\pi} \cdot A\Omega \cdot (QT) \text{ counts } s^{-1}$$

where A is the telescope area,

Ω the solid angle (field-of-view), and

QT is the product of the detector quantum efficiency and cumulative optical transmission.

The maximum aperture of the FOS will be 1.4 arc seconds, giving $\Omega = 4.61 \times 10^{-11}$ sr. Then, using $A = 4 \times 10^4 cm^2$ and an average QT = 0.03, the signal is

$$S = 4.4 \times 10^{-3} \text{ B counts } s^{-1},$$

or the sensitivity, s, is

$$s = \frac{S}{B} = 4.4 \times 10^{-3} \quad \text{counts } s^{-1} \ R^{-1}.$$

The specified noise and background count rate is of the order of 10^{-3} counts s^{-1}, so in principle, the detection of a source with a surface brightness of 1 Rayleigh is possible, but will require 6.3 hours for the accumulation of 100 counts (10% statistical uncertainty). Thus, ST will be incapable of providing significant ultraviolet information except for HI Ly α and OH, and the Ly α observations of both Halley and Tempel 2 will be adversely affected by geocoronal Ly α.

VI. Ultraviolet Instrumentation

A. Viewing geometry

The problem of defining the viewing geometry of a spectrographic instrument is a problem common to both planetary and cometary fly-by missions. Clearly this geometry should be optimized to the period of encounter when the planet or comet subtends its largest angular size, but it should also allow for significant observations during the cruise phase of the mission. For a cometary mission, this problem is further complicated by the nature of the gaseous coma; the comet appears different in size in the light of different constituents and this size changes with the heliocentric position of the comet. Moreover, the scale length differs markedly amongst the major constituents; $\sim 10^7$ km for H, $\sim 10^6$ km for C and O and $\sim 10^5$ km for OH. This large a variation in apparent size, coupled with the variation in size as the spacecraft approaches the comet probably mandates a scanning instrument. Nevertheless, there are advantages, especially for a mission of several years duration, to using an imaging spectrograph, and such an instrument is described below.

The primary observing mode for an ultraviolet spectrograph is one in which the spectrograph slit is projected onto the comet in such a way that the long dimension of the slit is parallel to the sun-comet line. This geometry gives the greatest sensitivity to variations in the intensity isophotes of neutral emitters that may result from solar radiation pressure or from the interaction with the solar wind. The brightness profiles calculated in Section IV neglect these effects and predict circular isophotes, although it

is known that this is not strictly true for the radicals observed in the visible part of the spectrum (Malaise, 1976). In the imaging spectrograph described below, spatial resolution is obtained along the length of the slit while a wide spectral range (1160-3200 Å) at moderately high spectral resolution ($\lambda/\Delta\lambda \approx 500$) is maintained.

B. Spectrograph

The optical system is shown schematically (though not to scale) in Fig. 10. The spectrograph is fed by an f/8 off-axis telescope whose field stop is the entrance slit of the spectrograph. This instrument is an echelle spectrograph employing a concave grating as a post-disperser. For the purpose of this exercise we will assume the ultraviolet detector to be a microchannel plate detector (MCP) with a suitable readout system to give a resolution of 100 x 100 pixels over an effective area of 20 x 20 mm^2. The details of the electronic readout system will not be given here but it should be noted that such a system is now within the state-of-the art of detector technology.

The principal instrument parameters are summarized in Table 4. We will confine our discussion to two areas of importance to a cometary mission -- spatial resolution and sensitivity. Fig. 11 shows the echellogram that would be produced on the detector face. Spectral dispersion is along the horizontal axis while spatial imaging of the entrance slit is along the vertical axis. There are 100 spatial elements in the 2 cm slit image. Note that none of the important comet features, shown on the figure, occur at the

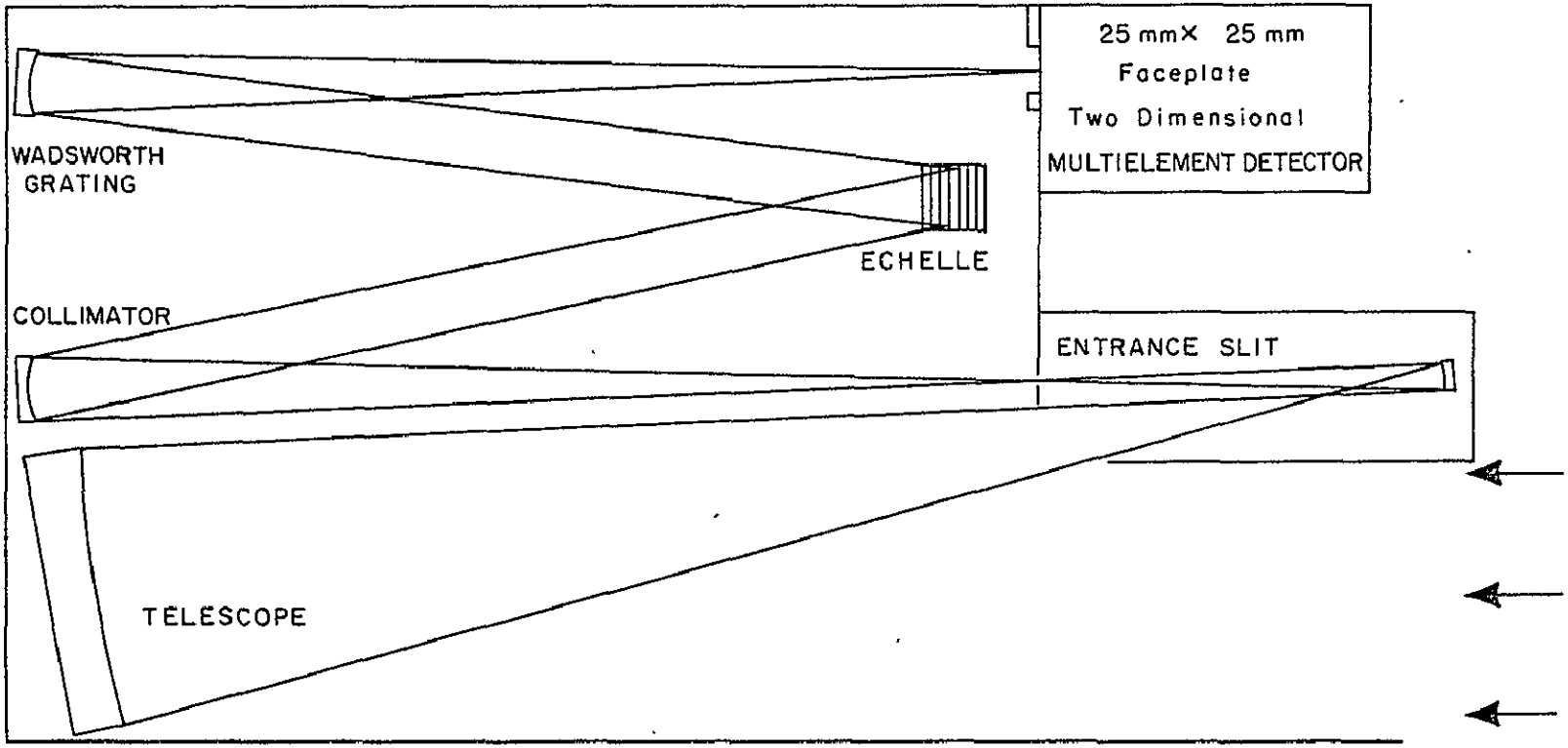

Figure 10. COMET FLY-BY / RENDEZVOUS ULTRAVIOLET SPECTROMETER SYSTEM

TABLE 4. Instrument Parameters

Telescope:	f/8 80 cm focal length
Spectrograph:	f/8 crossed dispersion echelle 80 cm focal length
Grating:	Echelle - 900 ℓ/mm, blaze angle 7.5° Post-disperser - 1250 ℓ/mm, blaze angle 1.6°
Spectral range:	1160-3200 Å in 7 orders
Detector:	20 x 20 mm^2 microchannel plate, 100 x 100 pixels
Spectral resolution:	$\lambda/\Delta\lambda$ = 500 ($\Delta\lambda$ = 6A at 3000A; 2.5A at 1250A)
Spatial resolution:	2.5 x 10^{-4}rad (20,000 km at 0.5 a.u.)
Sensitivity:	5 counts $s^{-1}kR^{-1}pixel^{-1}$

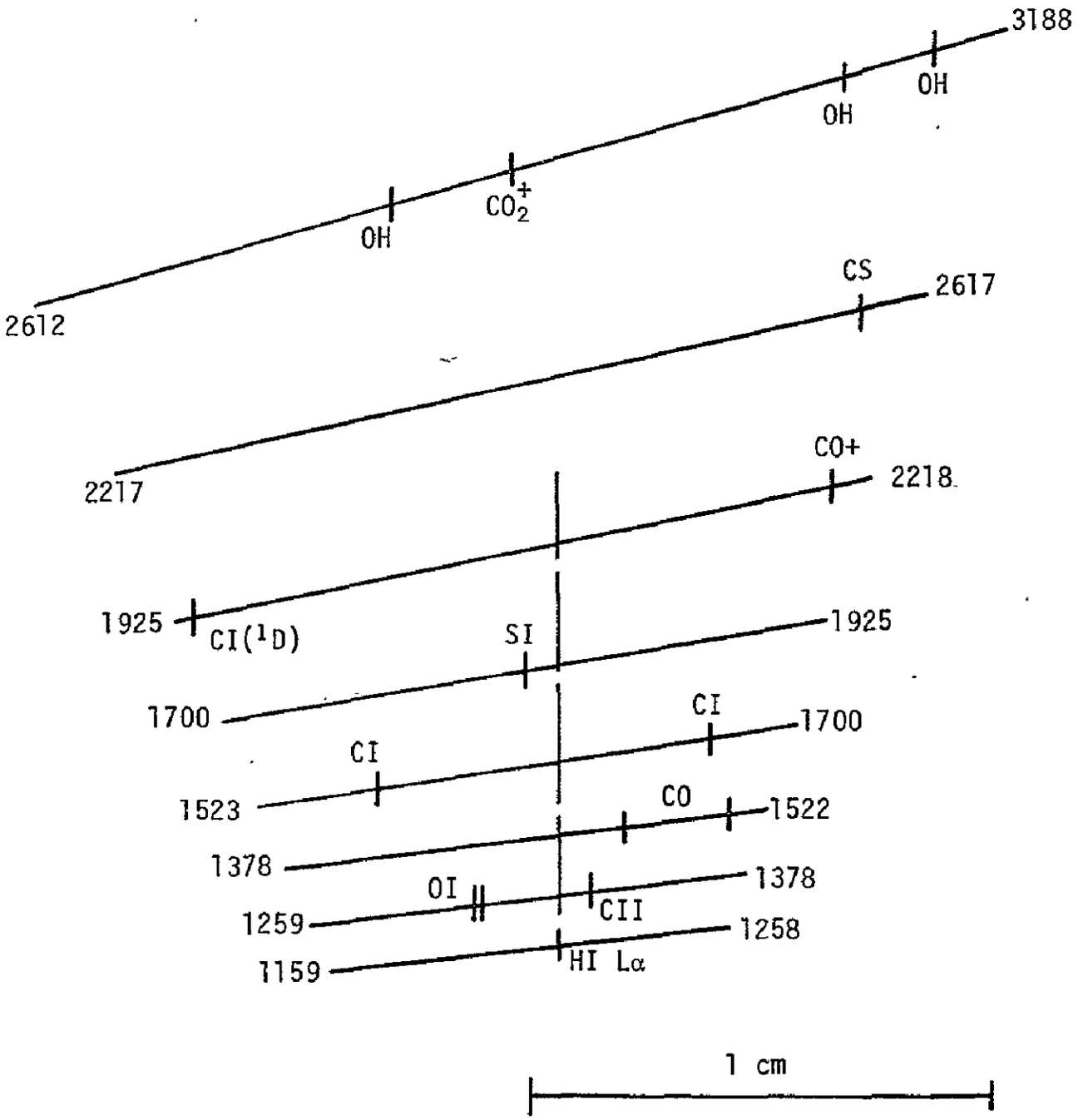

Fig. 11. Echellogram patterm. The wavelengths (in A) indicated are the half-intensity points of the single slit diffraction pattern of the grating in orders 5 - 12.

same diffraction angle. Thus the HI Lα image, if it extended across the entire slit, as indicated by the dashed line, would not mask any other spectral feature. In practise, the long wavelength orders would have to be filtered to prevent second order contamination from the post-disperser grating.

At the long wavelength end of the spectrum the separation between orders is ≈25 pixels, while in the vicinity of the CI 1657 multiplet the order separation is ≈11 pixels. At an observing distance of 0.5 a.u., each pixel is ≈20,000 km, so that the order separation corresponds to a linear distance at the comet of 5×10^5km and 2.2×10^5km, respectively. These distances are comparable with the scale lengths of these emission features. As the spacecraft approaches the comet, the linear distance corresponding to each pixel decreases and the image expands covering several spectral orders. However, no information is lost, as the spectral features remain well separated, until the total 2 cm slit length becomes smaller than the emission scale length. In the case of the Halley fly-by, at ±1 day from encounter the distance between the spacecraft and the comet is less than 0.05 a.u. and each pixel is less than 2000 km. At even closer distances the slit sees a source of uniform brightness and an enhanced signal/noise ratio can be obtained by summing the data from all of the pixels along the slit image at a given wavelength.

The sensitivity can be derived in a manner similar to what was done in Section V:

$$S = B \cdot \frac{10^6}{4\pi} \frac{A_g A_{pixel}}{F^2} (QT) \text{ counts } s^{-1}\text{pixel}^{-1}.$$

Here A_g is the grating area (100 cm^2),

A_{pixel} is the pixel area ($4 \times 10^{-4} cm^2$),

and F is the telescope focal length (80 cm).

In this case, we expect an average value of QT $\approx$0.01 over the spectral range, so that

$$S = 0.5\ B \cdot (QT) \approx 5 \times 10^{-3}\ B \text{ counts } s^{-1}\text{pixel}^{-1}.$$

The sensitivity is thus

$$s = \frac{S}{B} = 5 \times 10^{-3} \text{ counts } s^{-1}R^{-1}\text{pixel}^{-1}.$$

This result is similar to that derived in Section V for Space Telescope, except that now, since a cometary ultraviolet image will extend over several pixels, the counting statistics can be improved by summing these pixels although this results in a loss of spatial resolution. There is another important advantage over the use of Space Telescope in that during the cruise phase of a comet mission, a UVS will be free to make observations of the comet 24 hours a day over a period of a month or more while it is unlikely that this large a block of time would be available from ST.

The sensitivity derived above is comparable with that of the Voyager UVS (Sandel et al. 1978) except that it is achieved at much higher spectral resolution (e.g. $\Delta\lambda$ = 2.5A at λ = 1216A). This number is typical of current ultraviolet instrumentation suitable for interplanetary missions and it is not likely to be improved significantly in the next few years. The ultimate limit on sensitivity, ignoring HI Lα scattered by interplanetary hydrogen

and diffuse galactic background radiation, is set by detector noise induced primarily by cosmic rays. Assuming ≈10 events s^{-1} distributed over the detector area gives 10^{-3}counts s^{-1}pixel^{-1}. With this background, an emission of 1 Rayleigh would give a S/N of 2 in one pixel with a 1000 sec integration time, or a S/N of 4 in one hour. Thus, with exposures of ~1 day, and summing all available pixels, so that all spatial information is lost, we can probably achieve a limiting sensitivity of 0.1 R.

C. Dust Hazard

Dust emitted by the comet can have a serious effect on the primary optical surface of any ultraviolet experiment. Degradation can result from the impact of the dust particle regardless of whether or not it remains on the surface. To evaluate the possible hazard we again use models of dust production given by Newburn (1978). Since the dust is emitted radially outward from the comet, it is a potential hazard only when the primary optical element is observing towards the nucleus when the spacecraft is within ~10^6km of the comet center-of-mass. For the Halley fly-by at closest approach a UVS will probably only see solar UV radiation reflected from the dust coma which will probably saturate the instrument (e.g. reflected solar Lα from the moon is ≈50 kR). In this case the deployment of an optical shutter/dust cover might be desirable which would thus, eliminate the hazard. For a Tempel 2 rendezvous at 100 km from the nucleus, the optimum viewing direction for a UVS is outward through the coma, again removing the hazard.

Nevertheless, the dust models of Newburn indicate that dust is not a severe problem even if the nucleus were to be viewed directly. For Halley, he gives the total fluence on the spacecraft for a 10^3km closest approach as a function of dust particle size. By integrating the product of total fluence and particle cross-section over all particle sizes, we can find the fraction of total area impacted by dust particles during the entire fly-by. This turns out to be $<10^{-3}$ so that the degradation of exposed optical surfaces will be negligible.

For Tempel 2, Newburn gives the dust particle flux that the spacecraft will experience at a rendez-vous orbit of 100 km. In one second, the fractional area impacted is $\sim 3 \times 10^{-7}$ so that an exposed surface will be completely coated with a monolayer of dust in about 41 days. Again, this is not a serious problem as a UVS will not find much of interest looking directly at the nucleus. Thus it appears that dust is not a serious hazard for the proposed Halley/Tempel 2 mission and the need for the development of a space-qualified windshield wiper is eliminated.

VII. Conclusions

The results of the modelling of the ultraviolet coma have already been summarized at the end of Section IV, and we present only a brief review here. From the point of view of ultraviolet spectroscopy the proposed Halley/Tempel 2 mission is not very promising, since although H and OH, the dissociation products of H_2O, are detectable, the many other interesting ultraviolet emission features recently detected in the spectrum of Comet West, are at or below the sensitivity threshold of state-of-the-art ultraviolet instrumentation suitable for such a mission. The carbon model used is rather elementary and has yet to be verified by further observations (there have been no bright comets since West in 1976) but despite the uncertainties introduced by the model it is possible to identify the reasons for this guarded outlook. Both comets are to be observed at large distance from the sun (1.53 and 1.37 a.u., respectively) and the ultraviolet brightness varies roughly as r^{-6}. Furthermore, Comet Tempel 2 is just not an exciting comet in terms of gas evolution. Model calculations show that Comet Halley inside 1 a.u. and Comet Encke would both be more suitable targets within the existing capabilities of ultraviolet spectroscopic instrumentation.

APPENDIX A

A MODEL OF CARBON PRODUCTION IN A COMETARY COMA

(Astronomy and Astrophysics, November 1978)

I. INTRODUCTION

The recent detection of atomic carbon in the comae of two recent comets in comparatively large abundance relative to water (Feldman et al., 1974; Opal and Carruthers, 1977; Feldman and Brune, 1976) has raised several questions concerning the "parent" molecule source in the nucleus of the comet and the cosmogonic origin of this parent. The questions of relative abundance and origin in the solar nebula, however, may be premature if the production rates of the various species derived from the observations are not based on a proper physical and chemical description of the coma.

In the analyses of rocket ultraviolet spectra of Comets Kohoutek (1973 XII) and West (1976 VI) cited above, a simple Haser (1957) model, rigorously valid only for the case of where photodissociation dominates photoionization (such as occurs with H_2O) was used. Regardless of whether the ultimate carbon parent is CO or CO_2,* the observed carbon results from a break in the C-O bond brought about by solar extreme ultraviolet radiation and, as will be seen below, the dominant destruction mechanism for CO is photoionization, not photodissociation. Therefore, a large fraction of the neutral carbon observed results from the dissociative recombination of CO^+ with electrons. The evidence that this mechanism is important comes from the observed strong CI 1931 A line (Feldman and Brune, 1976) which results from resonance

*CH_4 appears to be excluded as the major parent of C in comet West on the basis of an upper limit to the H_2 production rate assuming $CH_4 + h\nu \rightarrow CH_2 + H_2$ with nearly 100% efficiency (Stieff et al., 1972).

scattering of sunlight from carbon atoms in the metastable ^1D state. This state is not likely to be excited in photodissociation (McElroy and McConnell, 1971) of CO. The radial profile of the carbon emission and the relative C and CO abundance is therefore related to the CO^+ concentration and will be sensitive to the details of the ion chemistry within the coma as well as to any effects of the solar wind interaction with the outer coma.

The problem is further complicated by the existence of large uncertainties in the values of the photodissociation and photoionization rates, J_d and J_i, respectively, which arise from uncertainties in the cross sections and relative yields to an extent that make the uncertainty in the solar EUV flux seem negligible. This uncertainty also affects the determination of the mean outflow velocity of the atomic fragments, which in most cases is 3 to 5 times that of the thermal outflow velocity of the parent. Finally, a significant error has been found in the atomic carbon lifetime used in previous papers (Feldman and Brune, 1976; Opal and Carruthers, 1977) which considerably lengthens the carbon atom lifetime and decreases the apparent carbon production rate relative to CO. The implication of this change is that only a given fraction of the CO^+ ions produced ultimately recombine, leaving a large number to survive into the tail.

Since the Haser model is clearly inadequate to a discussion of cometary carbon production, we have developed a one-dimensional radial outflow model of the dissociative recombination source, assuming a nucleus composed of H_2O and CO. In this model the excess velocity of the dissociation products is included, along with the finite lifetime of the $C(^1D)$ state and the effects

of thermalizing or deactivating collisions. Even though plasma effects which are likely to be important at distances greater than 10^5 km from the nucleus are not considered, the model gives good qualitative agreement with three recent comet observations: the ultraviolet fluxes of Feldman and Brune (1976); the radial carbon emission profile of Opal and Carruthers (1977); and the CO^+ and H_2O^+ column densities given by Wyckoff and Wehinger (1976).

II. PHOTODESTRUCTION RATES

Of primary importance to any coma model, the photodestruction rates J_i and J_d are obtained by integrating the product of solar flux and relevant cross section over all wavelengths shortward of the ionization or dissociation threshold. For molecules it is also necessary to know what fraction of the total absorption cross section leads to either dissociation or ionization. When discrete absorption is into predissociating states, this contribution to J_d must also be included but often this is not known. For CO and CO_2, the total absorption cross section between the dissociation and ionization limits at best gives an upper limit to the photodissociation produced in this wavelength range. At wavelengths shorter than the ionization limit, ionization is usually strongly favored over dissociation, but recently Lee et al. (1975) showed that the fluorescence yield in CO resulting from dissociation into excited atomic or atomic ion states could be as high as 20% near 300 Å.

To illustrate the difficulty with existing data, Table 1 shows the values of J_i and J_d for CO quoted by different authors plus a reevaluation

using the cross sections cited by Hudson (1971) and the solar fluxes of Donnally and Pope (1973). It should be noted (G. Schmidtke, private communication) that these fluxes are probably 50% low for moderate solar activity although they are probably reasonable for conditions of low solar activity ($F_{10.7}$=70-80) which prevailed at the times of the comet observations. Presumably all of these values were computed using the same basic spectroscopic data and with solar fluxes not differing by more than 50%. The present results for J_d are given in the table as extreme values depending on whether or not discrete absorption between 885 and 1116 A leads into predissociating states or not. For the model calculation the lower value (no predissociation) is used.

TABLE 1

CO PHOTODISSOCIATION AND PHOTOIONIZATION RATES AT 1 A.U.

Source	J_d (s^{-1})	J_i (s^{-1})
McElroy and McConnell (1971)	6.6×10^{-7}	-
Siscoe and Mukherjee (1972)	-	7.8×10^{-7}
Wyckoff and Wehinger (1976)	1.9×10^{-7}	2.7×10^{-7}
Ip and Mendis (1976)	1.0×10^{-7}	20×10^{-7}
McElroy et al.(1976)	-	12×10^{-7}
This work	$1.9\text{-}3.1 \times 10^{-7}$	4.5×10^{-7}

For atomic carbon, the photoionization cross section is difficult to measure directly and we must rely on theoretical values. The latest calculation, by Carter and Kelly (1976), is no more than 25% higher than that of McGuire (1968). The few experimental points that exist are indirectly determined, but agree with the calculated values to within a factor of two. The high value of J_i calculated by Johnson (1972) and quoted by Axford (1972) apparently arises from an error in the table of McGuire which gives a non-zero cross section at 1200 A, longward of the threshold for ionization from the $C(^3P)$ ground state at 1100 A. A more appropriate value for J_i is $6.0 \times 10^{-7} s^{-1}$, for low solar activity compared to $4.0 \times 10^{-6} s^{-1}$ quoted by Axford. With this lower value of J_i, it is now necessary to consider a contribution from charge-exchange ionization by solar wind protons to obtain the total ionization probability but, according to Huntress (1977), this is important only for the near resonant case of H^+ and O. Neglecting any charge exchange contribution gives a carbon lifetime of 1.67×10^6 s at 1 A.U. Carbon atoms in the ^1D state can also be photoionized by solar Lyman-α radiation, but this does not affect the lifetime of carbon atoms in the ground (^3P) state, and does not contribute significantly to the total carbon loss rate.

Taking these values into account, the results of Feldman and Brune (1976) have been revised in Table 2. The finite size of the instrument field-of-view has also been corrected for in the case of the CI λ 1657 and CO emission. The overall result is to lower the CO production rate from that given previously by a factor of 2 relative to that of water, $1.0 \times 10^{30} s^{-1}$, derived from the observed OH emission. The carbon atom production rates are in good agreement with Q_{CO}, in spite of considerable uncertainties in the values of g and τ and these numbers suggest that most of the carbon is

initially produced in the ^1D state, and that CO^+ recombination is probably the dominant source of C. Since CO is relatively long-lived, at large distances from the nucleus ($\sim 10^5$ km) a significant amount of CO^+ formation still occurs, but the ions are preferentially swept into the ion tail before they recombine. Thus the observed carbon gives only a lower limit to the production rate of its immediate parent.

TABLE 2

REVISED PRODUCTION RATES IN COMET WEST AT 0.385 A.U.

Species	τ (s) at 1 A.U.	Q (s^{-1})
$CO^\dagger$	1.4×10^6	2.6×10^{29}
C (total)†	1.67×10^6	1.9×10^{29}
C (^1D)	3.2×10^3 *	1.3×10^{29}

* independent of distance from sun.

† corrected for finite field of view.

III. ION MODEL

For the purpose of evaluating the recombination contribution to the carbon production rate it is necessary to have a model of the cometary ionosphere. The basic ion chemistry of a coma containing H_2O and CO has recently been described by Shimizu (1975) and by Ip and Mendis (1976). For the two observations being considered here, the gas production rate was

sufficiently high so that the mean free path of a CO^+ ion remains much smaller than the distance from the nucleus ρ even at distances of the order of 10^5 km. Thus, a steady state ion model should be sufficient.

For a given ion (X^+), the equilibrium equation at distance ρ is:

$$J_i(X)n(X) + \sum_j k_j n(X)n(M_j) = \alpha(X^+)n(X^+)n(e) + \sum_\ell k'_\ell\, n(X^+)n(M_\ell) \qquad (1)$$

where $J_i(X)$, the photoionization rate, is evaluated at heliocentric distance r taking into account absorption of solar EUV radiation in the neutral coma,

$n(X)$ is the abundance of species X,

$\alpha(X^+)$ is the dissociative recombination rate coefficient, in our case evaluated at T = 300°K,

k_j are the rate coefficients for ion-molecule reactions producing X^+, and

k'_ℓ are the rate coefficients for those reactions destroying X^+.

Diffusion of ions into the tail, probably significant for $\rho \gtrsim 10^5$ km is neglected.

The production rates of CO and H_2O, Q_{CO} and Q_{H_2O} respectively, are determined from the ultraviolet observations of CO and OH emission, and the density (e.g., of CO) at distance ρ from a nucleus of radius ρ_o is given by the Haser (1957) formula for the mother molecule:

$$n(CO) = \frac{Q_{CO}}{4\pi\rho^2 \bar{v}} e^{-\beta_{CO}(\rho-\rho_o)} \qquad (2)$$

Here Q_{CO} is in molecules s^{-1},

$\bar{v}$ is the mean outflow velocity, and

$\beta_{CO}^{-1} \equiv \bar{v}\tau_{CO}$, τ being the species lifetime.

With CO and H_2O as mother molecules it is necessary to consider only the ions CO^+, H_2O^+, HCO^+ and H_3O^+, the latter being the dominant ion at distances where H_2O remains abundant. The neutral daughters C, O, OH and H are computed using the Haser relation of Eq. (2). Equations of the form of (1) for each ion are solved iteratively for the four ions subject to the external condition of charge conservation, i.e., the electron density is forced to equal the total ion density. This requires the implicit assumption that the electrons are everywhere thermalized, an assumption that probably breaks down at the same values of ρ where plasma diffusion begins to dominate the CO^+ loss term. Since the dependence of α on electron temperature goes as $T_e^{-0.5}$, the result is relatively insensitive to the variation of T_e.

The reactions included in the model are listed, along with the reaction rates used, in Table 3. In practice, although there are several unknown reaction rate coefficients, only those involving the mother molecules are important, and laboratory data is available for them. The results of the ion model calculation are shown in Fig. 1 for the conditions of the Comet West observation. In this model $\bar{v}$ was taken to be 1 km s^{-1} and ρ_o = 10 km. Since CO is so much longer lived than H_2O, CO^+ is clearly the dominant ion for $\rho \gtrsim 10^4$ km.

IV. CARBON PRODUCTION

At a distance ρ, the density element of atomic carbon due to production of C at ρ' ($\rho' < \rho$) is given by:

TABLE 3

BASIC ION CHEMISTRY

Reaction	Rate Coefficient*	Reference
$H_2O + h\nu \rightarrow OH + H$	$J_d = 1.22 \times 10^{-5}$	a
$H_2O + h\nu \rightarrow H_2O^+ + e^-$	$J_i = 6.0 \times 10^{-7}$	a
$CO + h\nu \rightarrow C + O$	$J_d = 2.0 \times 10^{-7}$	b
$CO + h\nu \rightarrow CO^+ + e$	$J_i = 4.5 \times 10^{-7}$	b
$CO^+ + e \rightarrow C + O$	$\alpha(CO^+) = 3.0 \times 10^{-7}$	c
$H_2O^+ + e \rightarrow \begin{cases} OH + H \\ O + H_2 \end{cases}$	$\alpha(H_2O^+) = 1.0 \times 10^{-6}$	c
$H_3O^+ + e \rightarrow \begin{cases} OH + H_2 \\ H_2O + H \end{cases}$	$\alpha(H_3O^+) = 1.3 \times 10^{-6}$	d
$HCO^+ + e \rightarrow CO + H$	$\alpha(HCO^+) = 3.0 \times 10^{-7}$	d
$CO^+ + H_2O \rightarrow HCO^+ + OH$	$k_1 = 2.2 \times 10^{-9}$	e
$H_2O^+ + H_2O \rightarrow H_3O^+ + OH$	$k_2 = 1.7 \times 10^{-9}$	e
$H_2O^+ + CO \rightarrow HCO^+ + OH$	$k_3 = 1.0 \times 10^{-9}$	f
$HCO^+ + H_2O \rightarrow H_3O^+ + CO$	$k_4 = 2.7 \times 10^{-9}$	g
$H_3O^+ + C \rightarrow HCO^+ + H_2$	$k_5 = 2.0 \times 10^{-9}$	h

*J_d and J_i in s^{-1} at 1 a.u.

α_i and k_i in $cm^3\ s^{-1}$

References:

a. M. Festou, private communication

b. This work

c. Ip and Mendis (1976)

d. Leu et al. (1973)

e. Ferguson (1973)

f. Estimate

g. Huntress and Anicich (1976)

h. Herbst and Klemperer (1973)

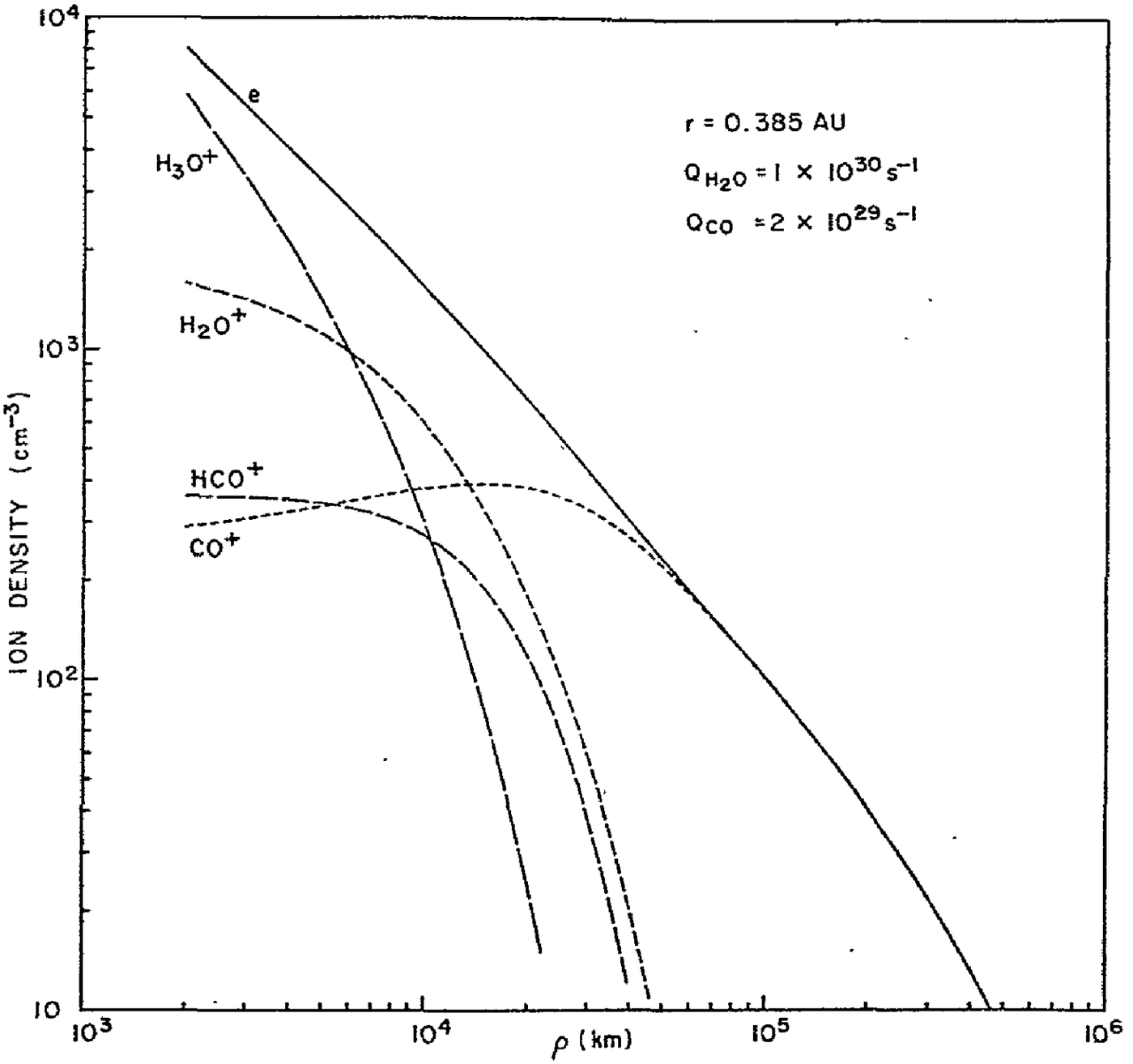

Fig. 1 Ion and electron densities in the steady-state ion chemistry model, evaluated for the conditions of the Comet West observation of Feldman and Brune (1976). Ion transport at large values of ρ has been neglected.

$$dn(C) = \frac{P(\rho')\rho'^2}{v'\rho^2} e^{-\beta_C(\rho-\rho')} d\rho' \qquad (3)$$

where $P(\rho')$ is the production rate per unit volume and v' is the mean velocity of the atomic fragment. We briefly consider the cases of photodissociation and dissociative recombination separately.

a. Photodissociation. Here $P = J_d(CO)n(CO)$ and all of the carbon atoms are assumed to be in the ^3P state. In the absence of collisions, as a result of energy conservation, these atoms would have a velocity $v' \tilde{\sim} 5$ km s^{-1}, which for simplicity is taken to be radially outward. Instead of defining a collision zone within which all atoms would be thermalized, different populations of atoms are defined, "slow" and "fast", as follows. The probability of an atom produced at ρ' escaping the coma without suffering a single collision is given by

$$p_{es}(\rho') = e^{-\sigma N(\rho')} \qquad (4)$$

where $N(\rho')$ is the total gas column density from ρ' to ∞ and σ is a mean total collision cross section, here taken to be 2.5×10^{-15} cm^2. Equation (3) then gives the contribution to the "fast" population:

$$dn_{fast}(C) = p_{es}(\rho')\, dn(C) \qquad (3a)$$

Consequently $$dn_{slow}(C) = dn(C) - dn_{fast}(C) \qquad (3b)$$

For the "slow" component $v' = 1$ km s^{-1}. The two components are evaluated separately at ρ by integrating Equations (3a) and (3b) up to $\rho' = \rho$.

b. Recombination. The possible final states energetically allowed are:

$$CO^+ + e \rightarrow C(^3P) + O(^3P) \quad (a)$$

$$C(^1D) + O(^3P) \quad (b)$$

$$C(^3P) + O(^1D) \quad (c)$$

In the analagous case of O_2^+ recombination, every reaction gives at least one $O(^1D)$ atom (Zipf, 1970) so that (a) may be neglected with respect to (b) and (c). The branching ratio between (b) and (c) is not known, and while a logical choice would be to make (b) and (c) equally probable, to fit the observed CI 1931 A emission from Comet West requires unity efficiency into (b). This value is adopted, recognizing that the factor of two uncertainty is consistent with most of the other uncertainties in the model. Because of the long (3200 sec) lifetime of the ^1D state collisional quenching is taken into account using the rate coefficient $k_Q = 2.0 \times 10^{-10} cm^3 s^{-1}$ appropriate to the quenching of $O(^1D)$ by H_2O (Streit et al., 1976). Those atoms that are collisionally deactivated to the ^3P state are added to the "slow" population. For the remainder the contribution to the $C(^3P)$ density is given by the production rate

$$P = \alpha(CO^+)n(e)n(CO^+) \cdot \frac{A_D}{A_D + k_Q n(H_2O)} \left[1 - \exp\left(\frac{-A_D(\rho - \rho')}{v''}\right)\right] \quad (5)$$

where A_D is the $(^1D - {}^3P)$ radiative transition probability and $v'' \approx 4$ km s^{-1} is the excess velocity of the $C(^1D)$ atoms.

The results of the calculation of atomic carbon density for the conditions of the Comet West observation are shown in Fig. 2. Note that the "slow" population from both photodissociation and recombination is dominant to

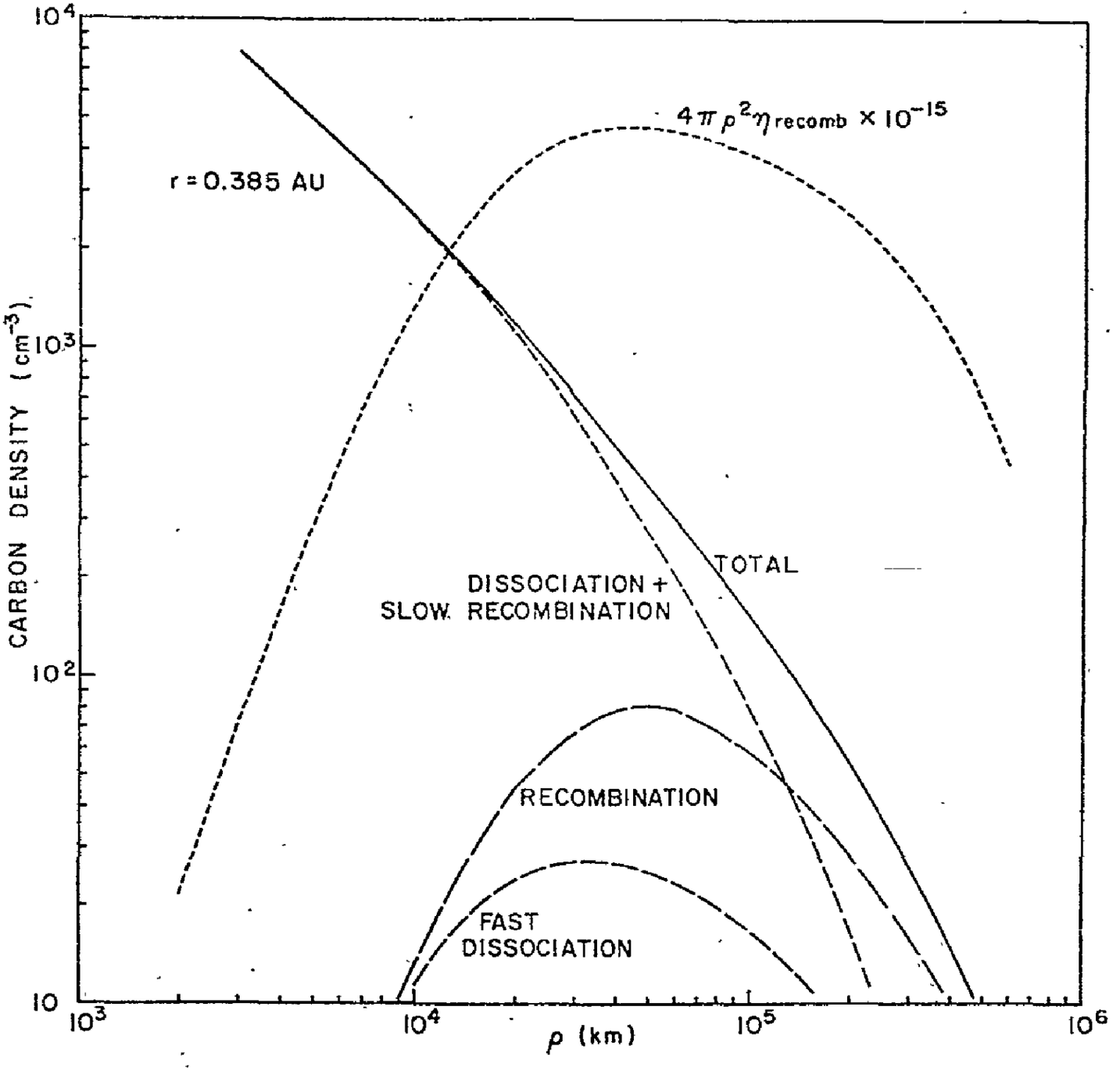

Fig. 2 Density of atomic carbon, evaluated for the same conditions as Fig. 1. The different velocity components are indicated. Also shown is the contribution at each value of ρ to the total $C(^1D)$ production rate.

nearly 10^5 km, giving a result similar to what is obtained with the simple Haser model. This is the result of the very large total gas production rate for this comet which gives rise to a very extended "collision zone".

An interesting comparison is given in Fig. 3 for the gas production rates derived from the observations of Comet Kohoutek of Opal and Carruthers (1977), which are some 3 to 4 times smaller than the values used in Fig. 2. The radius of the "collision zone" is reduced by about this same factor as can be seen by comparing the contribution from the "fast" component of photodissociation products for the two cases. As for the recombination contribution via $C(^1D)$, its importance is enhanced as the total gas production rate decreases and is likely to be dominant at larger values of heliocentric distance. However, in both cases the distribution of the carbon atoms produced this way as a function of radial distance ρ is quite similar, reflecting principally the CO^+ ion distribution in the coma, which is, in fact, similar for the two cases. The explanation for this effect is straightforward--in that region of the coma where the H_2O density is sufficiently high to collisionally deactivate $C(^1D)$ atoms, the CO^+ ions formed are converted to HCO^+ ions, also by collisions with H_2O. Thus recombination becomes a significant source of $C(^1D)$ only outside the "collision zone" where CO^+ is the principal ion and where recombination is the dominant ion loss mechanism. For $\rho \gtrsim 10^5$ km, the ion density becomes low enough so that diffusion of ions into the tail becomes important relative to recombination.

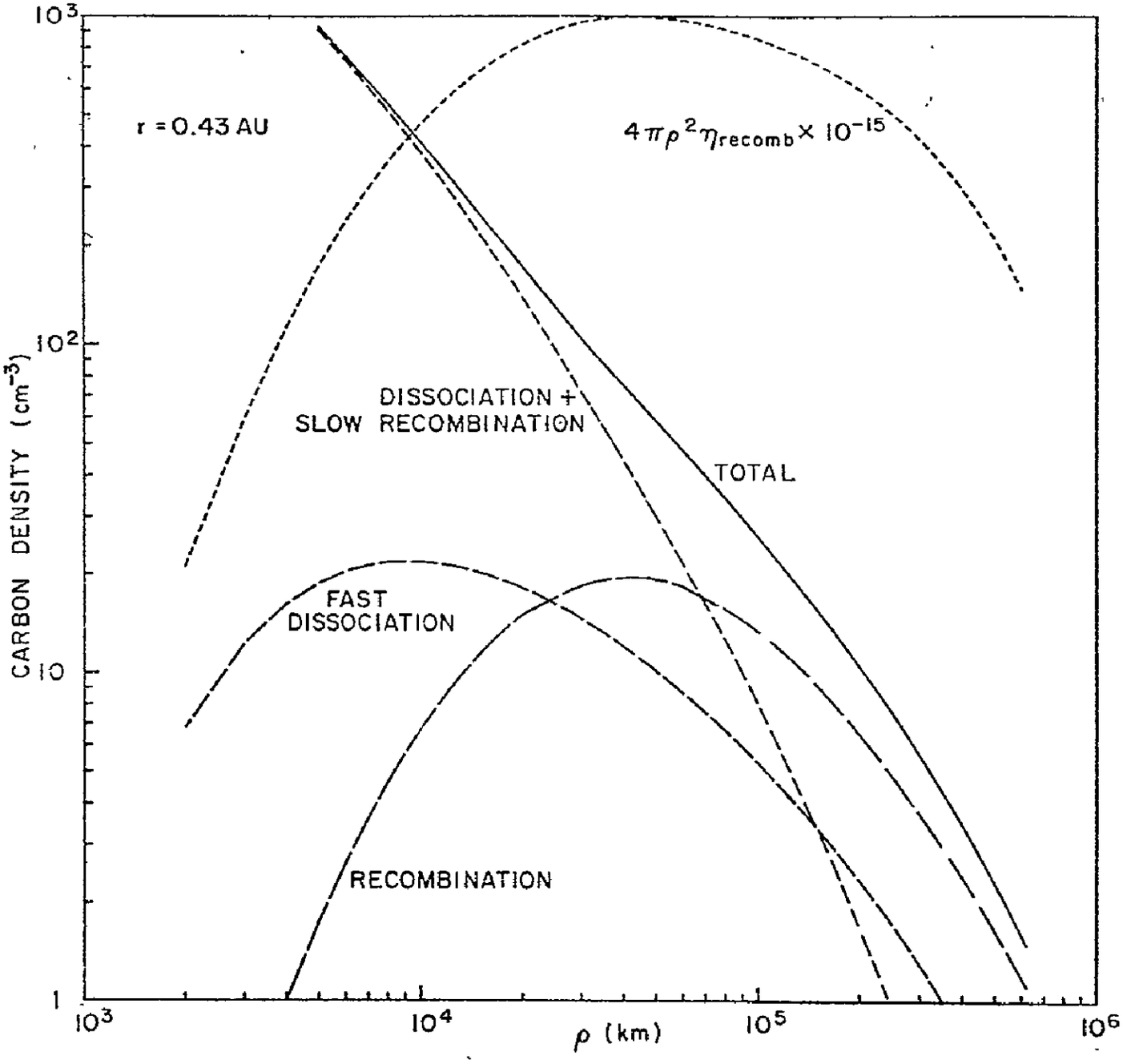

Fig. 3 Same as Fig. 2 for the conditions of the Comet Kohoutek observation of Opal and Carruthers (1977).

V. COMPARISON WITH OBSERVATIONS

Before embarking on a comparison of the results of this model with the available observational data, it should be reemphasized that one-dimensional models of the type described above are highly oversimplified approximations to the complex physical environment of the cometary coma. Not only are many of the basic parameters highly uncertain, but the one-dimensional nature of the model ignores important effects such as the spatial and velocity distributions of the atomic fragments produced through dissociation or recombination, the non-thermal nature of the electron distribution at distances from the nucleus where recombination (with a temperature dependent rate coefficient) is important, and ion transport into the tail due to radiation pressure and plasma diffusion. Even for the relatively straightforward case of radicals produced near the nucleus by photodissociation of minor parent molecules, Malaise (1976) has shown that the one-dimensional Haser model is inadequate to account for the observations. Moreover the data themselves do not give a completely consistent interpretation as, for example in Table 2 using the revised atomic carbon lifetime, the production rate of $C(^3P)$ is one-half that for $C(^1D)$ whereas the ^3P production rate should be greater than the ^1D rate. Perhaps it is sufficient to note that the model, developed to explain the observed $C(^1D)$ population, is in reasonable accord with the other observations.

a. $C(^1D)$ Production. The experiment of Feldman and Brune (1976) measures the total C I λ 1931 flux from which the total $C(^1D)$ production rate is

derived. The contribution to the total ^1D production rate from a shell of thickness $d\rho$ at ρ is shown in Figs. 2 and 3 for the two model cases described above. Again, note that this contribution has a maximum near $\rho = 3 \times 10^4$ km for both cases. Collisional quenching of ^1D atoms is significant only for $\rho < 10^4$ km, while ion transport probably dominates recombination as the principal CO^+ loss mechanism only for $\rho > 10^5$ km, so most of the $C(^1D)$ survives to its radiative lifetime and hence appears fairly abundant in the coma. For the Comet West observation, the model gives $Q(^1D) = 1.2 \times 10^{29}$ sec^{-1}, in excellent agreement with the value given in Table 2 even though both have uncertainties of at least a factor of two. Despite these caveats, the model clearly indicates that the observed $C(^1D)$ in the coma most likely results from dissociative recombination of CO^+ and electrons.

b. C I λ 1657 Brightness Profile. From their objective grating spectra of Comet Kohoutek, Opal and Carruthers (1977) derived a radial brightness profile of the C I λ 1657 emission with a spatial resolution of $\sim 1.1 \times 10^5$ km. Unlike the simultaneously observed O I λ 1304 emission, the carbon profile did not fit a simple one-component Haser model, and Opal and Carruthers argued that this implied two parents for the C atom, i.e., an ultimate grandparent of CO_2. Brightness profiles for models considered here were obtained by integrating the C density along a line-of-sight and the results for the Comet Kohoutek observation are shown in Fig. 4. For comparison, the predicted brightness profile for the Comet West observation of Feldman and Brune (1976) is also shown. The dissociation and recombination components are shown separately and it is evident that the resulting profile is different from the simple Haser

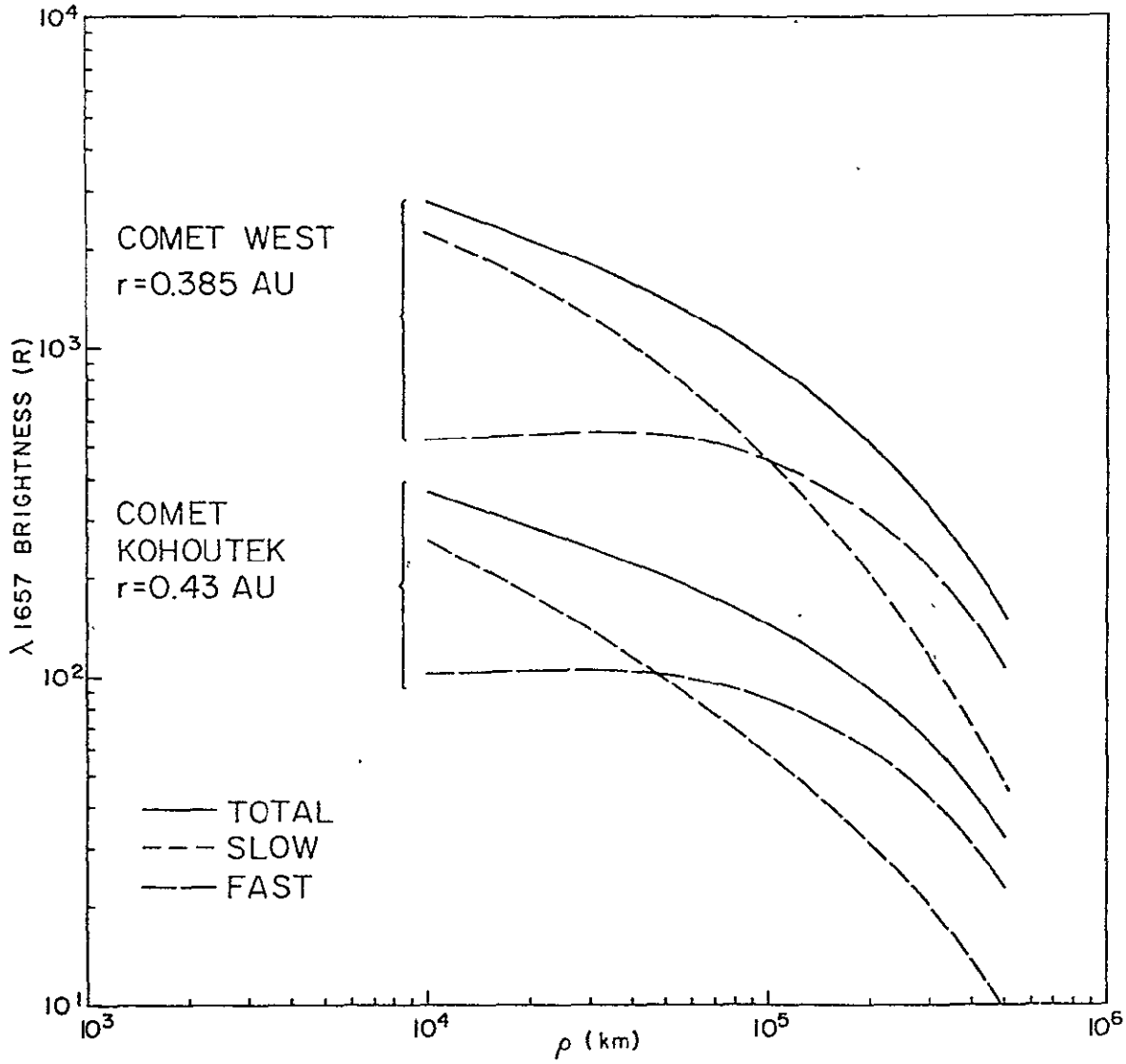

Fig. 4 Brightness profiles of the C I 1657 A emission derived by integrating the densities shown in Figs. 2 and 3 along a line-of-sight.

model in accord with the conclusions of Opal and Carruthers. Their data are not shown because of the problem of deconvoluting their instrument function from the published data. The most serious discrepancy appears to be for $\rho \gtrsim 3 \times 10^5$ km, where the observed brightness decreases more rapidly with ρ than does the model, but this may be an instrumental artifact since the brightness is weak and the derived value is very sensitive to the subtraction of an airglow background (C. B. Opal, private communication).

Opal and Carruthers noted that the carbon isophotes appeared to be circular. Since the recombination source of carbon atoms predominantly affects the outer isophotes, the circular symmetry implies nearly equal CO^+ densities at $\rho \gtrsim 3 \times 10^4$ km on both the sunward and anti-sunward sides of the coma. This may be interpreted to indicate that ion transport is still not an important CO^+ loss mechanism at this value of ρ as noted above.

c. $\underline{CO^+/H_2O^+ \text{ Abundance Ratio}}$. The relative ion column densities given by Wyckoff and Wehinger (1976) for Comet Kohoutek at 0.5 a.u. serve as a monitor of the ion model used in the calculation. They give a value of $\sim$100 for the column density ratio of CO^+ to H_2O^+ at $\rho = 1.0 \times 10^4$ km. In contrast, the model gives a value of 3 at $\rho = 1.0 \times 10^4$ km, but this number is increasing very rapidly with ρ to a value of 100 near $\rho = 5 \times 10^4$ km. However, the density ratio is a very sensitive function of the H_2O ionization lifetime and the smaller value of J_i $(2.0 \times 10^{-7} s^{-1})$ given by Giguere and Huebner (1978) produces a much better fit to the data of Wyckoff and Wehinger with no significant change to the carbon profiles.

Qualitatively, it is found that the CO^+/H_2O^+ ratio is twice as large in the Comet West model than in the Comet Kohoutek model. This is the result of the larger gas production rate in Comet West, and although H_2O^+ is produced initially more rapidly, the larger H_2O abundance results in a rapid conversion of H_2O^+ to H_3O^+. Thus, paradoxically, the H_2O^+ ion is more easily observed in a comet with a smaller H_2O production rate. This is in accord with the observations of H_2O^+ in both of these comets (P. A. Wehinger, private communication).

VI. CONCLUSION

The model described here is capable of satisfactorily explaining several new observations of recent bright comets. The C I λ 1931 emission provides direct evidence that dissociative recombination in the cometary ionosphere is a significant, if not the dominant, source of the carbon atoms observed in the comas of Comets Kohoutek and West. The model also bears directly on the question of whether CO or CO_2 is the ultimate parent of the atomic carbon and appears to favor CO since the high abundance of CO^+ needed to explain the derived $C(^1D)$ production rate does not seem attainable with a comet nucleus containing CO_2 rather than CO (Giguere and Huebner, 1978).

APPENDIX B

THE HASER MODEL

The model of Haser (1957) gives a simple expression for the density of a coma constituent resulting from the dissociation of a mother molecule. The model assumes isotropic production of the mother molecule, and radial outflow at a constant velocity. For the mother molecule this velocity is thermal, but for the products the excess kinetic energy (photon energy minus dissociation energy divided between the products so as to conserve linear momentum) must be added to the thermal energy.

The notation of Festou (1978) is adopted.

Then we have:

$$\beta_i^j = (\tau_i^j v_i)^{-1}$$

where i is either m (mother), r (daughter) or s (grandaughter);

j refers to the lifetime (τ) for dissociation (d),

ionization (i) or total (t), where

$(\tau^t)^{-1} = (\tau^d)^{-1} + (\tau^i)^{-1}$, and

v_i is the outflow velocity.

If ρ is the radial distance from the center of the nucleus, ρ_c the radius of the nucleus, then the region of the coma of interest is $\rho >> \rho_c$. Then, assuming $\beta_m^t \neq \beta_r^t \neq \beta_s^t$, the densities of the mother (n_m), daughter (n_r) and grandaughter (n_s) can be written in terms of the production rate Q_m of the mother in molecules sec^{-1}.

$$(1)\quad n_m(\rho) = \frac{Q_m}{4\pi\rho^2 v_m}\ \exp\ (-\beta_m^t \rho)$$

$$(2)\quad n_r(\rho) = \frac{Q_m}{4\pi\rho^2 v_r}\ \frac{\beta_m^d}{(\beta_r^t - \beta_m^t)}\ \left[\exp(-\beta_m^t\rho) - \exp(-\beta_r^t\rho)\right]$$

(Here the daughter is a dissociation product)

$$(3)\quad n_s(\rho) = \frac{Q_m}{4\pi\rho^2 v_s}\ \left[A\ \exp(-\beta_m^d\rho) + B\ \exp(-\beta_s^t\rho) + C\ \exp(-\beta_r^t\rho)\right]$$

$$\text{with } A = \frac{\beta_m^d}{(\beta_s^t - \beta_m^t)}\left[1 + \frac{\beta_m^t}{(\beta_r^t - \beta_m^t)}\right]$$

$$B = -A + \frac{\beta_m^d \beta_r^t}{(\beta_r^t - \beta_m^t)(\beta_s^t - \beta_r^t)}$$

and $C = -A - B$

Equation (2) is used to calculate the densities of H and OH produced by the photo-dissociation of water evaporating from the cometary nucleus, while equation (3) gives the density of H derived from OH. For the model calculations the following parameters were used (τ at 1 a.u.):

	$\tau^{-1}(\text{sec}^{-1})$	$v(\text{km sec}^{-1})$
H_2O	1.22×10^{-5}	1.0
OH from H_2O	7.5×10^{-6}	1.15
H from H_2O	5×10^{-7}	19.6
H from OH	5×10^{-7}	6.0

REFERENCES

Axford, W. I. 1972, in "Solar Wind", ed. C. P. Sonett et al., NASA SP-308 p. 609.

Bertaux, J. L., Blamont, J. E. and Festou, M. 1973, Astron. and Astrophys. 25, 415.

Carter, S. L. and Kelly, H. P. 1976, Phys. Rev. A, 13, 1388.

Carruthers, G. R., Opal, C. B., Page, T. L., Meier, R. R. and Prinz, D. K. 1974, Icarus, 23, 526.

Donnelly, R. F. and Pope, J. H. 1973, NOAA Technical Report ERL 276- SEL 25.

Feldman, P. D., Takacs, P. Z., Fastie, W. G. and Donn, B. 1974. Science, 185 705.

Feldman, P. D. and Brune, W. H. 1976, Astrophys. J. (Letters), 209, 145.

Feldman, P. D., Opal, C. B., Meier, R. R. and Nicolas, K. R. 1976. in "The Study of Comets", ed. B. Donn et al., NASA SP-393 p. 773.

Ferguson, E. E. 1973, Atomic Data Nucl. Data Tables, 12, 160.

Festou, M. 1978, Thèse de doctorat d'état, Université Paris VI.

Giguere, P. T. and Huebner, W. F. 1978, Astrophys. J., 223, 638.

Haser, L. 1957, Bull. Acad. Roy. Belgique, 43, 740.

Herbst, E. and Klemperer, W. 1973, Astrophys. J., 185, 505.

Hudson, R. D. 1971, Rev. Geophys Space Phys., 9, 305.

Huntress, W. T. 1977, Astrophys. J. Suppl., 33, 405.

Huntress, W. T. and Anicich, V. G. 1976, Astrophys. J., 208, 237.

Ip, W. H. and Mendis, D. A. 1976, Icarus, 28, 389.

Jenkins, E. B. and Wingert, D. W. 1972, Astrophys. J., 174, 697.

Johnson, H. E. 1972, Planet. Space Sci., 20, 829.

Keller, H. U. and Lillie, C. F. 1974, Astron. and Astrophys., 34, 187.

Keller, H. U. and Lillie, C. F. 1977, Astron. and Astrophys., 62, 143.

Lee, L. C., Carlson, R. W., Judge, D. L. and Ogawa, M. 1975, J. Chem. Phys., 63, 3987.

Leu, M. T., Biondi, M. A. and Johnsen, R. 1973, Phys. Rev., A7, 292.

Malaise, D. 1976, in "The Study of Comets", ed. B. Donn et al., NASA SP-393, p. 740.

McElroy, M. B. and McConnell, J. C. 1971, J. Geophys. Res., 76, 6674.

McElroy, M. B., Kong, T. Y., Yung, Y. L. and Nier, A. O. 1976, Science, 194, 1295.

McGuire, E. J. 1968, Phys. Rev., 175, 20.

Newburn, R. 1978, in Reports to the Comet Science Working Group, JPL.

Opal, C. B., Carruthers, G. R., Prinz, D. K. and Meier, R. R. 1974, Science, 185, 702.

Opal, C. B. and Carruthers, G. R. 1977, Astrophys. J., 211, 294.

Sandel, B. R., Shemansky, D. E. and Broadfoot, A. L. 1978, Nature, 274, 666.

Shimizu, M. 1975, Astrophys. and Space Sci., 36, 353.

Siscoe, G. L. and Mukherjee, N. R. 1972, J. Geophys. Res., 77, 6042.

Stieff, L. J., Donn, B., Glicker, S., Gentieu, E. P. and Mentall, J. E. 1972, Astrophys. J., 171, 21.

Streit, G. E., Howard, C. J., Schmeltekopf, A. L., Davidson, J. A. and Schiff, H. I. 1976, J. Chem. Phys., 65, 4761.

Whipple, F. L. 1950, Astrophys. J., 111, 375.

Wyckoff, S. and Wehinger, P. A. 1976, Astrophys. J., 204, 604.

Zipf, E. C. 1970, Bull. Amer. Phys. Soc., 15, 418.